Implications of population connectivity studies for the design of marine protected areas in the deep sea:

Taboada, Sergi; Riesgo, Ana; Wiklund, Helena; Paterson, Gordon; Koutsouveli, Vasiliki; Santodomingo, Nadia; Dale, Andrew; Smith, Craig; Jones, Daniel; Dahlgren, Thomas G.; Glover, Adrian

Published in:
Molecular ecology

Publication date:
2018

Implications of population connectivity studies for the design of marine protected areas in the deep-sea: an example of a demosponge from the Clarion-Clipperton Zone

Sergi Taboada[1,2,*], Ana Riesgo[1], Helena Wiklund[1], Gordon L.J. Paterson[1], Vasiliki Koutsouveli[1], Nadia Santodomingo[1], Andrew C. Dale[3], Craig R. Smith[4], Daniel O.B. Jones[5], Thomas G. Dahlgren[6,7,8] and Adrian G. Glover[1]

[1]*Life Sciences Department, The Natural History Museum, Cromwell Road, London, UK*

[2]*Departamento de Ciencias de la Vida, Ecología y Ciencias Ambientales, Universidad de Alcalá, Alcalá de Henares, Spain*

[3]*The Scottish Association for Marine Science, Oban, UK*

[4]*Department of Oceanography, University of Hawaii, Honolulu, Hawaii*

[5]*National Oceanography Centre, University of Southampton Waterfront Campus, Southampton, United Kingdom*

[6]*NORCE, Uni Research, Bergen, Norway*

[7]*Department of Marine Sciences, University of Gothenburg, Sweden*

[8]*Gothenburg Global Biodiversity Centre, University of Gothenburg, Sweden*

*Corresponding author: *sergiotab@gmail.com*

Key words: Central Pacific; deep-sea mining; polymetallic nodules; conservation genetics; phylogeography; oceanographic modelling

Abstract The abyssal demosponge *Plenaster craigi* inhabits the Clarion-Clipperton Zone (CCZ) in the north-east Pacific, a region with abundant seafloor polymetallic nodules with potential mining interest. Since *P. craigi* is a very abundant encrusting sponge on nodules, understanding its genetic diversity and connectivity could provide important insights into extinction risks and

design of marine protected areas. Our main aim was to assess the effectiveness of the Area of Particular Environmental Interest 6 (APEI-6) as a potential genetic reservoir for three adjacent mining exploration contract areas (UK-1A, UK-1B and OMS-1A). As in many other sponges, *COI* showed extremely low variability even for samples ~900 km apart. Conversely, the 168 individuals of *P. craigi,* genotyped for 11 microsatellite markers, provided strong genetic structure at large geographical scales not explained by isolation by distance. Interestingly, we detected molecular affinities between samples from APEI-6 and UK-1A, despite being separated ~800 km. Although our migration analysis inferred very little progeny dispersal of individuals between areas, the major differentiation of OMS-1A from the other areas might be explained by the occurrence of predominantly northeasterly transport predicted by the HYCOM hydrodynamic model. Our study suggests that although APEI-6 does serve a conservation role, with species connectivity to the exploration areas, it is on its own inadequate as a propagule source for *P. craigi* for the entire eastern portion of the CCZ. Our new data suggest that an APEI located to the east and/or the south of the UK-1, OMS-1, BGR, TOML and NORI areas would be highly valuable.

Introduction

The Clarion-Clipperton Zone (CCZ), a vast area located in the equatorial NE Pacific, encompasses a broad range of habitats, including abyssal hills, seamounts, fracture zones, and extensive abyssal plains, as well as strong gradients in export flux (Wedding et al. 2013). Abyssal plains of the region can contain high concentrations of polymetallic nodules (potato-sized concretions of manganese, iron, cobalt, copper and nickel), with sediments around nodules typically consisting of a mixture of well oxygenated siliceous oozes and deep-sea clays (Mewes *et al.* 2014). Importantly, these polymetallic nodules provide a great abundance of hard substrate for sessile organisms and appear to support faunal communities distinct from nearby abyssal soft sediments (Mullineaux 1987; Thiel *et al.* 1993; Smith & Demopoulos 2003; Veillette *et al.* 2007; Amon *et al.* 2016; Vanreusel *et al.* 2016). In fact, epifaunal densities are significantly higher in areas with dense nodule coverage, with some major taxa such as alcyonacean and antipatharian corals being virtually absent from nodule-free areas (Vanreusel *et al.* 2016).

The nodule-rich CCZ represents the most important area for deep-sea mining exploration worldwide (an actual exploration area of ca. 6 million km^2; Lodge *et al.* 2014), with mining operations potentially to be initiated by 2025 (Smith & Demopoulos 2003; Glover & Smith 2003; Smith *et al.* 2008a). Small-scale impact experiments conducted so far in the CCZ suggest that the local environmental impacts of nodule mining will be substantial (Borowski & Thiel 1998; Thiel *et al.* 2001; Smith *et al.* 2008b; Miljutin *et al.* 2011; Jones *et al.* 2017), and will directly affect abyssal epifauna (Amon *et al.* 2016; Vanreusel *et al.* 2016). Importantly, mining may not only impact areas where nodules are removed, but will aslo disturb adjacent areas through re-deposition from sediment plumes, potentially impacting larger seafloor areas than those directly affected by nodule removal (Oebius *et al.* 2001; Smith *et al.* 2008a). The long-term effects of this sediment re-deposition is not understood. These issues were central to the establishment by the International Seabed Authority (ISA) of a network of representative protected areas, termed Areas of Particular Environmental Interest (APEIs), across the CCZ, where exploration and mining activities are prohibited (Wedding *et al.* 2013). The CCZ is characterized by gradients in environmental conditions (e.g., surface-productivity and export flux, depth, and sediment

characteristics; ISA 2010) along an east-west and also a north-south axis, leading to marked variation in nodule size and coverage, but also changes in faunal composition along these gradients (Glover *et al.* 2002; Smith *et al.* 2008a; Wedding *et al.* 2013). The APEI network was designed accordingly, preserving the gradients of faunal distribution reflecting the biogeography and connectivity of marine benthic fauna across the region (Wedding *et al.* 2013).

To maximise protection of biodiversity over broad areas, like the CCZ, an understanding of biogeography, at both the species and community levels, is crucial (Wedding *et al.* 2013). To achieve this, the evaluation of species' ranges and their levels of population connectivity and turnover are needed (Baco *et al.* 2016). Efforts to determine the population genetic connectivity in deep-sea invertebrates have mainly been focused on chemosynthetic environments (Vrijenhoek 2010; Taylor & Roterman 2017). However, as stated by Taylor & Roterman (2017) in their recent review, the ephemeral nature and non-equilibrium conditions characteristic of these particular habitats could limit their comparability to other more common and stable deep-sea habitats. Molecular connectivity of marine invertebrates in non-chemosynthetic deep-sea habitats has barely been assessed and two recent reviews on this topic (Baco *et al.* 2016; Taylor & Roterman 2017), concluded that there is a clear need to assess the connectivity of deep-sea organisms from a variety of habitats, life history types, taxonomic groups, and depth zones. This is especially true for studies at abyssal depths and deeper since, to date, there is only one genetic study of species occurring below 5,000 m depth (Ritchie *et al.* 2017). For the CCZ very little information is available on the biogeography and connectivity of fauna inhabiting this region (Glover *et al.* 2002; Paterson *et al.* 2015; Janssen *et al.* 2015). Despite the prominent occurrence of nodules (*i.e.* hard substrate) in this abyssal region, the majority of connectivity studies conducted in the CCZ have focused on selected infaunal taxa (annelids and crustaceans) living in the sediment (e.g. Paterson *et al.* 1998; Glover *et al.* 2002) and with only a few using a molecular approach (Smith *et al.* 2008b; Janssen *et al.* 2015).

The recently-described abyssal demosponge *Plenaster craigi* Lim & Wiklund, 2017 (Lim et al., 2017) appears to be a good model species to assess the molecular connectivity and to establish biogeographic patterns from local to large spatial scales within the CCZ for a number

of reasons (Taboada *et al.* 2017). *Plenaster craigi*, potentially endemic to the central abyssal Pacific, is a remarkably common encrusting element of the nodule fauna, highly (or perhaps totally) dependent on nodules that provide the substrate where adults live attached (Lim *et al.* 2017). Thus, populations of this organism will surely be eliminated from the mined areas as nodules will be removed or become buried by sediment plumes. As filter-feeders, these organisms are likely to be vulnerable to sediment plumes generated in the water column after mining, as suggested by studies on shallow-water sponges (Schönberg 2016). Also, although nothing is known about its reproductive traits, *P. craigi* may be like most other sponges and it is assumed to have a limited dispersal phase through lecithotrophic larvae, with most larvae spending short periods of time in the water column– usually less than two weeks (see Maldonado 2006). So this species may have relatively limited dispersal ability compared to species with planktotrophic development.

Here we present the first study on the molecular connectivity and dispersal capabilities of an abyssal sessile invertebrate, the sponge *P. craigi*, from four different areas in the eastern CCZ: the APEI-6 area and three sampling sites within adjacent exploration contract areas UK-1 [UK-1 Stratum A (UK-1A), UK-1 Stratum B (UK-1B)], and Oceans Minerals Singapore OMS-1 Stratum A (OMS-1A) (Fig. 1A). The aim of this study is to assess whether APEI-6 may serve as a genetic reservoir and source of propagules for *P. craigi* if the above-mentioned exploration areas are disturbed by mining in the future. A fragment of the mitochondrial cytochrome *c* oxidase subunit I –*COI*– and 14 microsatellite markers previously isolated and characterized (Taboada *et al.* 2017) were used to assess the connectivity of the populations of *P. craigi*. In addition, oceanographic models were applied to investigate their relationship with connectivity patterns observed.

Material and methods

Sample collection, preservation and sampling design

A total of 180 specimens of the demosponge *P. craigi* were collected from four different areas within the CCZ: APEI-6 and UK-1A, UK-1B and OMS-1A (Table 1). UK-1A and UK-1B correspond to the UK exploration contract area while OMS-1A corresponds to the Oceans Minerals Singapore exploration contract area (Fig. 1). Samples were collected during three different oceanographic cruises: ABYSSLINE AB01 cruise (Oct 3–27, 2013), which studied the UK-1A and UK-1B areas on board the RV *Melville*, ABYSSLINE AB02 cruise (Feb 12–Mar 25, 2015) exploring the OMS-1 area on board the RV *Thomas G Thompson*, and MIDAS-JC120 cruise (April 15–May 19, 2015) exploring the APEI-6 area on board the RRS *James Cook*. The separate specimens of *P. craigi* were found attached to polymetallic nodules primarily collected using a USNEL type boxcore (0.25 m^2), but additionally from multicore, Brenke epibethic sledge, Agassiz trawl, and a ROV (Table 1). Sample and specimen handling followed the protocol in (Glover *et al.* 2015). Nodules were carefully observed individually under the stereoscope and once the sponges were found they were photographed; sponges were then removed from the nodule with a scalpel or forceps, preserved in either 80–95 % ethanol or RNA*later*, and immediately stored at -20ºC until DNA extraction.

Due to proximity between some of the samples collected in the different sampling sites some of the samples from the different areas were pooled together (*i.e.* APEI-6_Flat1 to APEI-6_Flat8 as APEI-6_Flat; APEI-6_Ridge1 to APEI-6_Ridge6 as APEI-6_Ridge; APEI-6_Trough1 to APEI-6_Trough4 as APEI-6_Trough; APEI-6_Deep1, APEI-6_Deep2 and APEI-6_Nodule as APEI-6_Deep-Nodule; UK-1A_BC06 and UK-1A_EB03 as UK-1A_BC06-EB03; UK-1A_BC08 and UK-1A_BC05 as UK-1A_BC08-BC05; UK-1B_BC06 and UK-1B_MC25 as UK-1B_BC06-MC25; UK-1B_BC18 and UK-1B_MC13 as UK-1B_BC18-MC13; UK-1B_EB09 and UK-1B_BC04 as UK-1B_EB09-BC04; OMS-1A-EB06, OMS-1A-BC11, and OMS-1A-BC08 as OMS-1A-EB06-BC11-BC08; OMS-1A-BC25, OMS-1A-MC23 and OMS-1A-BC26 as OMS-1A-BC25-MC23-BC26). Original sampling sites collected during oceanographic cruises

are found in Table 1 and pooled sampling sites considered in this study are shown in Table 2. Thus, a total of four areas and 30 different populations were identified in our study (Table 1–2).

Body size of P. craigi

Prior to DNA extraction, all preserved organisms were photographed in the lab using a Zeiss AxioCam Hrc camera attached to a stereoscope. The maximum length and maximum width of complete individuals were measured using the software AxioVision. These measurements were made to test whether there was any link between body size and (i) apparent cohorts inferred from the molecular analyses or (ii) different ecological variables. Linear correlation analysis between maximum length and maximum width using R (https://www.r-project.org/) indicated a moderate adjusted R-squared coefficient (R^2 = 0.473) and significant correlation between variables ($p < 0.05$); thus we used maximum length as the variable for size-frequency distributions. The correlation between maximum length vs. maximum width was plotted in R. One-way analyses of variance (ANOVAs) were conducted on maximum length using StatPlus vs 6 (www.analystsoft.com) (1) using sample areas (APEI-6, UK-1A, UK-1B and OMS-1A) as factors, (2) within APEI 6 using the four different sampling stations as factors (APEI-6_Flat, APEI-6_Ridge, APEI-6_Trough and APEI-6_Deep), and (3) between samples assigned to cluster 1 from the APEI-6 and UK-1A areas (see Results below). The Tukey-Kramer post-hoc test implemented in StatPlus was used to identify significant pairwise differences between areas.

DNA extraction and genotyping

Genomic DNA was extracted from a portion of tissue (approx. 1 mm^3) of each of the 180 individuals collected from the four different areas using the Tissue and Blood Qiagen extraction kit (Qiagen, www.qiagen.com) following the protocol provided by the manufacturer to a final elution of 100 µL. Prior to genotyping using microsatellites, we amplified and sequenced a fragment of the gene cytochrome *c* oxidase subunit I –*COI*– using the primers PorCOI2fwd and PorCOI2rev (Xavier *et al.* 2010) from a selection of 65 individuals from the four different areas (Supplementary Table S1). This *COI* fragment includes the Erpenbeck's 'I3-M11' fragment

(Erpenbeck *et al.* 2006), which has shown to be suitable to address intraspecific variability in other sponges (e.g. López-Legentil & Pawlik 2009; Xavier *et al.* 2010). Each PCR reaction mix contained a 21 µL of Red Taq DNA Polymerase 1.1x MasterMix (VWR), 1 µL (10 µM) of each primer and 2 µL of DNA extraction of each individual. For DNA amplification, the following PCR protocol was used [94 ºC/5 min – (94 ºC/1 min – 55 ºC/1 min – 72 ºC 1 min) x 38 cycles – 72 ºC/5 min]. Sequencing was conducted on an ABI 3730XL DNA Analyser (Applied Biosystems) at the Natural History Museum –NHM– molecular labs using the primers (forward and reverse) mentioned above.

Owing to the low intraspecific variability observed in the *COI* fragment (see Results), we genotyped all individuals using the 14 microsatellite loci (1Ple, 2Ple, 3Ple, 4Ple, 5Ple, 6Ple, 8Ple, 11Ple, 12Ple, 13Ple, 14Ple, 16Ple, and 19Ple) described by Taboada *et al.* (2017), using the PCR conditions described therein. The sizes of the fluorescently labelled PCR products were estimated using GeneScan 500 LIZ (Applied Biosystems, Foster City, CA, USA) on an Applied Biosystems 3130xl DNA analyser at the NHM molecular labs. Allele peaks were checked and edited using Geneious vs 8.1.7 (Kearse *et al.* 2012) before being placed into amplicon size "bins" and exported for analysis. Genotyping failed in 12 individuals (11 from APEI-6 and 1 from UK-1A) and thus results reported below for microsatellite analysis refer to 168 individuals from a total of 30 sampling stations (Table 1, 2).

In order to test for the occurrence of cryptic species between organisms from cluster 1 and the rest of specimens (see Population differentiation in Results section for details about cluster assignation), apart from using the information from the I3-M11 fragment, we sequenced a fragment of *28S* rRNA of a random selection of nine individuals assigned to the two different clusters (Supplementary Table S1). Primers used were 28Sa and 28Srd5b (Giribet *et al.* 2002; Schwendinger & Giribet 2005), and DNA amplification followed the PCR protocol [95 ºC/5 min – (95 ºC/1 min – 55 ºC/1 min – 72 ºC 1 min) x 38 cycles – 72 ºC/10 min]. Sequencing was conducted on an ABI 3730XL DNA Analyser (Applied Biosystems) at the NHM molecular labs using the primers mentioned above. Additionally, we performed a spicule analysis of a selection

of four individuals of these sequenced specimens to inspect for morphological differences (see Spicule Analysis section below).

Genetic diversity in P. craigi *populations*

Tests for linkage disequilibrium were performed using Genepop through probability tests for each pair of loci in each population with the level of significance determined by the following Markov chain parameters: 5,000 dememorization steps, 1,000 batches and 5,000 iterations per batch. Significance was adjusted by a false discovery rate method (Benjamini & Yekutieli 2001). Since three of the microsatellites appeared to be in linkage disequilibrium (see Results), all results refer to a total of 11 microsatellites.

Number of alleles (*Na*), number of private alleles (*Pa*), *e*stimations for the observed (*Ho*) and expected (*He*) heterozygosity, and the fixation index (F_{IS}), commonly used as an inbreeding coefficient, were performed using GenAlEx 6.5 (Peakall & Smouse 2006, 2012). Genetic (gene) diversity was calculated with GENODIVE vs 2.0b23 (Meirmans & Van Tienderen 2004) although for comparative purposes with other studies we will use *He* as a measure for genetic diversity. We used Genepop web version 4.2 (Raymond & Rousset 1995; Rousset 2008) to obtain values for departure from Hardy–Weinberg equilibrium (HWE) by locus and population (sampling site) using a probability test with level of significance determined by the following Markov chain parameters: 5,000 dememorization steps, 1,000 batches and 5,000 iterations per batch. Significance was adjusted by a false discovery rate method (Benjamini & Yekutieli 2001). These descriptors for the genetic diversity were calculated for the different sample sites separately and grouping samples into the four different areas. Additionally, these descriptors were also computed for the different areas considering samples of cluster 1 and cluster 2 separately.

Population differentiation in P. craigi

In order to test for population differentiation in *P. craigi* we used *COI* sequences from a selected number of individuals (65) from the four different areas (Supplementary Table S1) and genotyped 11 microsatellites for a total of 168 individuals (Table 1). *COI* overlapping sequence fragments

were assembled into consensus sequences using Geneious vs. 8.1.7, and aligned using Q-INS-I option of MAFFT (Katoh *et al.* 2002). The *COI* alignment was used to construct an un-rooted haplotype network with the program PopART (http://popart.otago.ac.nz) using the TCS network option (Clement *et al.* 2000).

Fragments of *28S* sequenced to test for the occurrence of cryptic species were assembled and aligned as described above for *COI*.

To examine evidence of clonality, multilocus genotypes of the 168 individuals studied here were compared in GenAlEx 6.5 (Peakall & Smouse 2006, 2012) using the 'Multilocus/Matches' function, which outputs a list of pairwise comparisons and the number of differing locus genotypes ignoring missing data. After confirming the absence of clones and also the lack of evidence of cryptic speciation (see Results), we performed four different methods to assess population structure and differentiation in the 168 individuals of *P. craigi* using the 11 microsatellites: two of these methods used a clustering approach (STRUCTURE and the discriminant analysis of principal components –DAPC–) and the other two were based on distances (F_{ST} estimations and the analysis of the molecular variance –AMOVA–).

Clustering methods. Samples were assigned to genetically homogenous populations (K) inferred using a Bayesian clustering algorithm without prior geographical information with the program STRUCTURE 2.3.4 (Pritchard *et al.* 2000). An admixture model was used with correlated allele frequencies and 150,000 MCMC iterations (burn-in of 50,000), repeated 10 times for each value of K from 1 to 30. The most likely value of K was determined using Evanno's *ad hoc* ΔK statistic (Evanno *et al.* 2005) calculated and plotted using Structure Harvester web v0.6.94 (Earl & vonHoldt 2012). The 10 replicates of optimal K were aligned using the *FullSearch* algorithm in the software package CLUMPP v1.1.2 (Jakobsson & Rosenberg 2007), then visualized using DISTRUCT v1.1 (Rosenberg 2004). STRUCTURE was also run, using the same specifications mentioned above, considering members of cluster 1 and cluster 2 separately.

We also performed Discriminant Analysis of Principal Components –(– with the *adegenet* package (Jombart 2008) implemented in R. DAPC defines clusters using the clustering algorithm

k-means on transformed data with principal component analysis. The algorithm k-means is then run sequentially with increasing values of k, and different clustering solutions are compared using the Bayesian Information Criterion. The number of principal components giving rise to the model with the highest predictive capacity were inferred with the cross-validation optimisation procedure using 100 replicates and the default parameters. The optimal cluster solution should correspond then to the lowest value of root mean squared error. We applied the DAPC analysis for: (i) the complete matrix of all samples grouped in the four different regions (APEI-6, UK-1A, UK-1B and OMS-1A) and in the 30 different sites; (ii) the complete matrix of all samples grouped by the cluster 1, the APEI-6 and UK-1A without samples assigned to cluster 1, UK-1B and OMS-1A; (iii) APEI-6, UK-1A and UK-1B after removing from the analysis samples from cluster 1 and all samples from OMS-1A; (iv) samples of APEI-6 and UK-1A belonging to cluster 1; and (v) cluster 2 samples, which included samples of the four different regions (APEI-6, UK-1A, UK-1B and OMS-1A) without members of cluster 1.

Distance methods. Population differentiation was estimated with the F_{ST} statistic between pairwise sampling sites using an infinite allele model in Arlequin vs 3.0 (Excoffier *et al.* 2005). Significance of F_{ST} values was evaluated by performing 20,000 permutations and corrected based on the false discovery rate method (Benjamini & Yekutieli 2001). Pairwise F_{ST} values grouping all samples by area were also estimated using the same specifications mentioned above. MICRO-CHECKER 2.2.3 (Van Oosterhout *et al.* 2004) was used to detect the presence of null alleles, error scoring owing to stuttering or large allele dropout and error. As the presence of null alleles in well-differentiated populations is known to yield an overestimation of population differentiation (Chapuis & Estoup 2006), we repeated our analysis excluding loci suggesting presence of null alleles. In all cases, the corrections only affected the second or third decimal place in the F_{ST} value for the pairwise comparisons between areas (not affecting significance of values) and consequently the effect of presence of null alleles was disregarded. Significance of F_{ST} values was also calculated for the different areas considering samples of cluster 1 and cluster 2 separately.

An Analysis of Molecular Variance (AMOVA) was used to determine the hierarchical distribution of genetic variation. To run this analysis, we grouped the sites in the different areas (APEI-6, UK-1A, UK-1B and OMS-1A). The significance of the AMOVAs was calculated with 20,000 permutations of the original data in the program Arlequin. Additionally, AMOVA was also calculated for the different areas considering samples of cluster 1 and cluster 2 separately.

Spicule analysis

We checked spicule composition of three individuals of cluster 1 (APEI-6_Flat.16, UK-1A.7, UK-1A.8) and one from cluster 2 (APEI-6_Flat.14). A small piece of tissue of the different specimens was first digested in nitric acid using a hotplate and subsequently washed twice with distilled water. Spicules were cleaned in absolute ethanol, mounted on a stub and coated with gold/palladium. Images of spheroxyasters were taken using a Zeiss Ultra Plus field emission scanning electron microscope at the NHM Imaging and Analytical Centre (IAC).

Dispersal patterns in P. craigi

Isolation by distance (IBD). A Mantel test (100,000 permutations) was performed in GENODIVE to test IBD using the whole data set of 168 individuals from the 30 populations and also using only a subset of individuals not including individuals from cluster 1 (see Population differentiation in Results). Geographical distances between sites were estimated using GENODIVE using the coordinates for every site. These distances were log-transformed and correlated to Slatkin's linearized pairwise F_{ST} estimates (F_{ST}/1-F_{ST}).

Detection of last-generation migrants. We performed a population assignment analysis calculating the likelihood ratio thresholds for the populations grouped in the four areas (APEI-6, UK-1A, UK-1B and OMS-1A) based on the Monte Carlo test with an α of 0.002 and 1000 replicated data sets using GENODIVE. This method assigns or excludes reference populations as possible origins of individuals on the basis of multilocus genotypes. Genetic assignment methods allow inferring where individuals originated, providing estimates of real-time dispersal through

the detection of immigrant individuals. The detection of last-generation migrants was performed in GENODIVE using a random 0.005 frequency (estimated to outperform tests) in 4,000 permutations. This test provides the likelihood of an individual belonging to a given population.

Migration patterns among areas. Effective population size (expressed as $\Theta=4Ne\mu$) and migration (M) were estimated with a Bayesian approach as implemented in LAMARC vs 2.1.10 (Kuhner 2006). Following suggestions by Kuhner (2006) we randomly reduced sample sizes for each area to 15 in order to increase run efficiency. Default values were used for effective population size and migration parameters. We performed Bayesian analyses with five replicates with 10 initial chains of 5,000 MCMC each, burn-in period of 1,000, and two final chains of 100,000 MCMC each with a burn-in period of 1,000. Three simultaneous heating searches (1, 1.1, and 2) were performed per replicate. LAMARC infers approximate credibility intervals (CIs) around most probable estimates (MPE) for each parameter. Parameter conversion was verified by examining stationarity in parameter trends over the length of the chains and Effective Sample Sizes (ESS) parameter using TRACER vs 1.6 (http://beast.bio.ed.ac.uk/Tracer). We interpreted ESS values > 250 as an indication that sampled trees were not correlated and thus represent independent simulations. Number of immigrants per generation per area was calculated using Θ and M (ΘM). LAMARC analyses were also run for members of cluster 1, selecting randomly 15 individuals from each area (APEI-6 and UK-1A).

Directionality of recent migration patterns was obtained with the diveRsity package in R (https://diversityinlife.weebly.com/), which uses the method described in Sundqvist *et al.* (2016) to plot the pairwise relative migration levels between populations from microsatellite allele frequency data. The sampling sites were pooled into the four different areas (APEI-6, UK-1A, UK-1B, and OMS-1A). We used the statistic *Nm* (*i.e.* the effective number of migrants), a more generally suitable measure of migration (Sundqvist *et al.* 2016), with a bootstrap of 10,000. However, since the method is still in experimental stages, results should be interpreted with caution. Additionally, migration patterns using diveRsity were also calculated for the different areas considering samples of cluster 1 and cluster 2 separately.

Detection of genetic breaks and correlation with geographical discontinuities. The occurrence of possible barriers determining the genetic structure of *P. craigi* populations was evaluated using the software BARRIER v2.2 (Guerard & Manni 2004). This program links a matrix of geographical coordinates with their corresponding distance matrix (F_{ST}), and applies the Fnier's maximum distance algorithm to identify a desired number of 'barriers' to gene flow among sites (*i.e.* zones where genetic differences between pairs of sites are the largest). This was done using the whole data set of 168 individuals from the 30 populations and also using only a subset of individuals not including individuals from cluster 1 (see Population differentiation in Results).

Modelling of larval dispersal by currents

The passive transport of larvae was simulated within a 9-year (Oct 2008–Sept 2017) record of daily velocity fields from the GOFS 3.0 1/12° global analysis of the HYCOM hydrodynamic model (Chassignet *et al.* 2007). A fourth order Runge-Kutta advective scheme was used with a 1-day timestep and a random horizontal diffusive component (diffusion coefficient k_x=1 m^2s^{-1}) representing unresolved scales of motion. In the absence of detailed understanding of larval behaviour and vertical positioning, transport was simulated within the horizontal model layer at 3,500 m depth, representing the lower water column at a level that is largely unobstructed by topography. Modelled currents at this depth are weak (the mean instantaneous current speed in a box encompassing the sample sites is 2.2 cm s^{-1}, and the mean residual flow speed, the mean of the underlying mean flow, is 0.5 cm s^{-1}; Aleynik *et al.* 2017). Larval connectivity between sites X and Y (the four different areas in our study) was assessed by continuously releasing 'particles' (1,000 per day) from site X throughout the first 4 years of the record, and determining the probability that they pass within a 25 km radius of site Y at any time within the following 5 years. Advection over this timescale should not be interpreted as representing the dispersal of a single larval generation, but as representing the cumulative dispersal of multiple generations, albeit represented as a single continuous pathway, so there is an implicit assumption that suitable benthic habitat exists along the pathway.

The reproductive effort of adults (determining timing and number of larvae in the water column), and the larval development and behaviour, determine how larvae interact with currents and ultimately influence the timing, distance and trajectory of larvae among habitats (Hilario *et al.* 2015). Sympatric shallow-water sponges may substantially differ in their timing for sexual reproduction and these differences appear to be related to changes in seawater temperature (Riesgo & Maldonado 2008). To our knowledge, the only work studying seasonality in relation to sexual reproduction in deep-sea sponges was conducted in the North Atlantic and concluded that the reproduction of *Radiella sol* Schmidt, 1970 was not asynchronous and remained at a constant low level, while *Thenea abyssorum* Koltun, 1964 showed highly synchronized gametogenesis and was linked to seasonal pulses of particulate organic carbon (Witte 1996). Since the flux of phytoplankton to deep-sea waters in the equatorial Pacific appears to be quasi-continuous, albeit with phytodetrital pulses (Smith *et al.* 1996), we assumed that, similarly to *R. sol* and in the absence of any reproductive data in *P. craigi*, the sponge studied here may have a constant low level of reproduction throughout the year.

Evaluating bottleneck events & population decline

We tested for recent effective population size reductions (bottlenecks) based on allele data frequencies using the software BOTTLENECK vs. 1.2.02 (Cornuet & Luikart 1996). This software assumes that "populations that have gone through a recent reduction of their effective population size show a reduction of the allelic diversity and heterozygosity, even though the allele frequencies are reduced faster than the heterozygosity" (Cornuet & Luikart 1996). The statistical analyses using a "sign test" (Cornuet & Luikart 1996) and a "Wilcoxon sign-rank test" (Luikart & Cornuet 1998) can be applied when more than 5 (but less than 20) loci are included, and we selected only the two most extreme models of mutation: infinite allele model (IAM) and the stepwise mutation model (SMM).

Results

I3-M11, 28S and spicule analyses

Grouping of samples in cluster 1 (see Population differentiation section below for details about assignation to individuals to clusters), with specimens showing high molecular affinities despite being several 100's km apart, made us suspect about the occurrence of cryptic species in our samples. Thus, a combination of molecular (*28S* and *COI* sequences) and morphological (spicules) analyses were conducted in a selection of individuals to detect the occurrence of cryptic species within our samples.

Although we found variability in the *COI* I3-M11 partition in the 65 individuals analyzed, these differences were not congruent with the two main clusters (cluster 1 and cluster 2) detected in our population genetic analysis using microsatellites (see below). Thus, we could not assign any haplotype to any putative cryptic species. Similarly, the fragment of 421 bp of *28S* from a total of nine individuals (four from cluster 1, including two samples from APEI-6 and two samples from UK-1A; five from cluster 2, including two samples from APEI-6, two from UK-1A and one from OMS-1A; Supplementary Table S1) showed no differences at all.

For the spicule analysis we focused on the comparison of spheroxyasters since these spicules were the only ones displaying some morphological variability. We observed no significant differences among spicules coming from organisms in cluster 1 and cluster 2, either in their size or in the number of rays per spicule (Supplementary Material Figure 1). The number of rays did not differ significantly between individuals of the two clusters, ranging from 14–30 for organisms from cluster 1 and 16–26 for organisms from cluster 2. However, there were slight differences in the ratio number of rays with spines between the two clusters; in cluster 1 the average was 89 % of rays with spines, whilst in cluster 2 it was 51 %. The size and features observed in spheroxyasters analysed here match those described in the original description of *P. craigi*, with a range of 11.2–13.1–15.4 µm for organisms in cluster 1 and 12.1–13.7–15.5 µm for cluster 2 (Lim *et al.* 2017). Importantly, the specimens used for the original description of the species by Lim *et al.* (2017) were collected in the OMS-1A area.

Body size of P. craigi

Correlation between maximum length and maximum width in *P. craigi* individuals measured here is shown in Supplementary Figure S2. Mean maximum length varied significantly between the different areas, with maximum lengths ranging from 3624±1265 μm (mean±S.D.) in APEI-6 to 5133±1776 μm in UK-1B (Fig. 2, Table 3, Supplementary Table S2). Tukey-Kramer post-hoc tests identified significant differences between APEI-6 samples and UK-1A and UK-1B samples (the former being significantly smaller than the two latter), and also between OMS-1A and UK-1B samples (the former being significantly smaller than the latter) (Figure 2, Table 3). Significant differences were also found between individuals assigned to cluster 1 from APEI-6 and UK-1A areas (Table 3), although no significant differences were found between Cluster 1 vs Non-Cluster 1 samples from the two different areas. No significant differences were detected for any pairwise comparison from the four different sampling stations within APEI-6 (APEI-6_Flat, APEI-6_Ridge, APEI-6_Trough, and APEI-6_Deep).

Genetic diversity in P. craigi *populations*

Three of the 14 loci (4Ple, 6Ple, and 8Ple) used in our analysis showed significant linkage disequilibrium (LD) in pairwise comparisons with other loci. After removing these three loci from the analysis, none of the pairwise comparisons showed significant LD. Thus, all the subsequent analyses describing the genetic diversity and population differentiation in *P. craigi* are based only on 11 loci (1Ple, 3Ple, 11Ple, 13Ple, 12Ple, 14Ple, 16Ple, 5Ple, 19Ple, 10Ple, and 2Ple) out of the 14 microsatellites originally characterized by Taboada *et al.* (2017).

Genotypic variation, measured by the percentage of differences between multilocus genotypes in pairwise comparisons between the 168 *P. craigi* samples, showed no identical genotypes (*i.e.* absence of clonality). The total number of alleles per population ranged from 12 in UK-1B_BC02 to 114 in APEI-6_Flat, with most of the variation resulting from three hypervariable microsatellites (*i.e.* 3Ple, 12Ple, and 16Ple; see Table 2, Supplementary Table S3). The mean number of alleles per population ranged from 1.091 to 10.364 in UK-1B_BC02 and APEI-6_Flat, respectively (Table 2, Supplementary Table S3). When considering the populations

grouped within the four main areas (APEI-6, UK-1A, UK-1B and OMS-1A), the total number of alleles ranged from 146 in OMS-1A to 172 in UK-1A, while the mean number of alleles ranged from 13.273 in both UK-1B and OMS-1A to 15.636 in UK-1A (Table 2, Supplementary Table S3). Private alleles were not present in all populations and ranged from 1 (mean number of private alleles = 0.091) in seven populations in the UK-1B and OMS-1A areas (UK-1B_BC17, UK-1B_BC20, UK-1B_BC02, UK-1B_BC03, OMS-1A-EB06-BC11-BC08, OMS-1A-BC12, and OMS-1A-BC10) to 10 (mean number of private alleles = 0.909) in UK-1A_BC12 (Table 2, Supplementary Table S3). Private alleles were present in all areas and ranged from 9 (mean number of private alleles = 0.727) in APEI-6 to 26 (mean number of private alleles = 2.364) in UK-1A (Table 2, Supplementary Table S3). When grouping samples from cluster 1 and cluster 2, the total number of alleles was 98 in APEI-6 and 103 in UK-1A for cluster 1, and ranged from 111 in APEI-6 to 146 in both UK-1B and OMS-1A for cluster 2 (Supplementary Table S4). The mean number of alleles was 8.909 in APEI-6 and 9.364 in UK-1A for cluster 1, and ranged from 10.091 in APEI-6 to 13.273 in both UK-1B and OMS-1A for cluster 2 (Supplementary Table S4). Private alleles were 29 in APEI-6 (mean number of private alleles = 0.704) and 34 in UK-1A (mean number of private alleles = 0.814) for cluster 1, and ranged from 11 (mean number of private alleles = 1.000) in APEI-6 to 33 (mean number of private alleles = 3.000) in OMS-1A for cluster 2 (Supplementary Table S4).

Genetic diversity (*He*) values varied widely across populations, ranging from 0.170 in UK-1B_BC02 to 0.705 in APEI-6_Flat, in part due to the relatively low number of individuals present in some populations (Supplementary Table S3). Genetic diversity was less variable across areas and ranged from 0.728 in UK-1B and OMS-1A to 0.791 in UK-1A (Supplementary Table 3). Inbreeding coefficient values (F_{IS}) were positive, resulting from heterozygosity deficit, for all the populations in the APEI-6 area and also for the majority of populations in the other three areas indicating non-random mating between individuals (Table 2). A few populations in UK-1A, UK-1B and OMS-1A showed negative F_{IS} values because of an excess of observed heterozygotes (Table 2). When considering the four large areas, F_{IS} values were always positive (Table 2). Several populations in the four different areas showed significant deviation from HWE, and when

considering the four areas together HWE deviations were detected in all of them (Table 2). When loci possibly affected by presence of null alleles (3Ple, 10Ple, 11Ple and 19Ple) were removed from the analysis, some of the populations showed no departure from HWE; however, the four different areas still showed a significant departure from HWE (Table 2). When grouping samples from cluster 1 and cluster 2, *He* values were 0.677 in APEI-6 and 0.712 in UK-1A for cluster 1, and ranged from 0.712 in UK-1A to 0.728 in both UK-1B and OMS-1A for cluster 2 (Supplementary Table S4). F_{IS} values were always positive and HWE deviations were detected for all the areas in cluster 1 and cluster 2 (Supplementary Table S4).

Population differentiation in P. craigi

Mitochondrial markers. A fragment of 526 bp of *COI* was analysed for 65 individuals of *P. craigi* occurring in the four different areas (Supplementary Table S1). Only two haplotypes were inferred in the haplotype network: H1 was the most common haplotype (accounting for 97 % of the total number of individuals) and occurred in individuals from the four areas (Figure 3); and H2, differing only in one mutational step from H1, was only present in two individuals from the UK-1A, namely UK-1A.4 and UK-1A.23 (Figure 3).

Microsatellites. The optimal number of populations for the whole data set obtained by the program STRUCTURE recovered two genetically homogeneous groups (k = 2) followed by three groups (k = 3) (Figure 4A). Results for k = 2 revealed two populations with no clear pattern of geographic subdivision: (i) cluster 1 (Orange group) included most of the samples in APEI-6_Flat, all the samples in UK-1A_BC08-BC05 and UK-1A_BC03 and a few samples in the stations UK-1A_BC06-EB03 and UK-1A_BC10; and (ii) cluster 2 (Blue group) contained the rest of the samples from APEI-6 and UK-1A, and all the samples from the sites in UK-1B and OMS-1A (Figure 4A). Results for k = 3 revealed substructure in cluster 2, with three populations of individuals present in different proportions in the four areas (Figure 4A). When grouping samples from cluster 1 and cluster 2, the optimal number of populations detected was two genetic groups (k = 2) for cluster 1, and three (k = 3) for cluster 2 (Supplementary Figure S3A-B).

DAPC analysis considering all the samples grouped in the four areas showed APEI-6 and UK-1A as the most similar areas, UK-1B being closer to UK-1A, while OMS-1A was the most divergent of the areas (Fig. 4B); a similar picture could be observed when analysing the 30 different sites separately (Supplementary Figure S3C). When the samples of the cluster 1 were separated and considered as a separated area, UK-1B and the remaining samples of APEI-6 and UK-1A grouped together, while samples from cluster 1 and OMS-1A appeared as the most divergent ones (Fig. 4C). After removing from the analysis all the samples from cluster 1 and OMS-1A area, DAPC showed differences between APEI-6, UK-1A and UK-1B, with samples from UK-1A and UK-1B more closely related than with APEI-6 (Supplementary Figure S4). When grouping samples from cluster 1, two groups with a significant overlap were detected in samples from APEI-6 and UK-1A (Supplementary Figure S3D). When grouping together samples from cluster 2, DAPC showed that APEI-6 and UK-1B samples were the most similar ones, with UK-1A being closer to UK-1B, and OMS-1A being again the most divergent area (Supplementary Figure S3E).

When treating all locations separately, F_{ST} values were significant for: (i) the majority of pairwise comparisons between APEI-6_Flat and UK-1A_BC08-BC05 with the rest of sampling sites; (ii) for UK-1B_BC18-MC13 with UK-1B_BC03 and the majority of OMS-1A sampling sites; (iii) OMS-1A_BC25-MC23-BC26 with three of the four sites of APEI-6 and three sites of UK-1A and UK-1B; and (iv) for five of the pairwise comparisons between APEI-6_Ridge with OMS-1A sites, amongst other comparisons (Supplementary Table S5). However, our F_{ST} values for locations treated separately should be interpreted with caution due to the low number of specimens analysed in some populations. When grouping samples per area, F_{ST} values ranged from 0.00709 between APEI-6 and UK-1A to 0.11132 between APEI-6 and OMS-1A, and were significant between all pairwise comparisons except for the comparison between APEI-6 and UK-1A (Table 4). F_{ST} values based only in the 7 microsatellites not affected by null alleles showed the same significant pairwise comparisons as with the whole set of microsatellites (Supplementary Table S6). When grouping samples from cluster 1, F_{ST} value was 0.011 and not significant between APEI-6 and UK-1A, while when considering samples from cluster 2 all

pairwise comparisons resulted significant except for the comparisons between APEI-6 and UK-1B, and between UK-1A and UK-1B (Supplementary Table S7).

Population differentiation using AMOVA, found significant differences between the four different areas, and also among populations within areas, among individuals within populations, and among all individuals, with the last representing the greatest source of variation (Table 5). When grouping samples from cluster 1, no significant differences were found between APEI-6 and UK-1A (Supplementary Table S8); for cluster 2, significant differences were found between the four different areas, among individuals within areas, and within individuals, with the last one representing the greatest source of variation (Supplementary Table S8).

Dispersal patterns in P. craigi

The Mantel tests detected no significant IBD when considering the whole data set of individuals ($p = 0.131$) and still was not significant after removing from the analysis individuals from cluster 1 (Orange group) ($p = 0.373$), which indicates that the genetic structure observed might be related to other processes (*e.g.* oceanographic currents, see below).

When considering the whole data set of individuals and setting two major barriers *a priori*, the barriers or genetic discontinuities appeared, in decreasing order of importance, between: (a) all the samples of the APEI-6 area plus three UK-1A sites (UK-1A_BC06-EB03, UK-1A_BC08-BC05, and UK-1A_BC14) and the rest of sites; and (b) most of the samples from OMS-1A (OMS-1A_BC21, OMS-1A_BC22, OMS-1A_BC09, OMS-1A_BC23, OMS-1A_BC25-MC23-BC26, and OMS-1A_BC10) and the rest of sites (Supplementary Figure S5). When removing cluster 1 from the analysis, the barrier between APEI-6 and UK-1A disappeared, and the three main barriers inferred appeared between (a) most of the OMS-1A sites (OMS-1A_BC10, OMS-1A_BC25-MC23-BC26, OMS-1A_BC23, OMS-1A_BC09, OMS-1A_BC22, and OMS-1A-BC21) and the rest of sites; (b) UK-1B_EB09-BC04 and UK-1B_BC02; and (c) OMS-1A-EB06-BC11-BC08, OMS-1A-BC12, and OMS-1A-BC07 (Supplementary Figure S5). Thus, after removing cluster 1 from the analysis the main barriers appeared to be between OMS-1A and the rest of the sites studied here.

The population assignment showed remarkable genetic exchange between areas, especially for APEI-6 and UK-1A with almost 50 % of their individuals inferred to come from UK-1A and UK-1B, and from APEI-6 and UK-1B, respectively (Supplementary Figure S6). In contrast, most of the individuals from UK-1B (73 %) and OMS-1A (97 %) were inferred to result from self-recruitment (Supplementary Figure S6). Only one last generation migrant was detected, an individual from UK-1A_BC14 (one of the southernmost sites in UK-1A; Fig. 1) that was inferred to come from UK-1B. Migration inferred using LAMARC showed no clear pattern of gene flow among the four different areas, with relatively low and similar numbers of immigrants per generation among the different pairwise comparisons; similar results were detected after analysing migration between APEI-6 and UK-1A from cluster 1 (Table 6–7). Migration directionality among areas using diveRsity detected significant migration both from OMS-1A and UK-1B to UK-1A (Figure 6F), and no significant migration directionality was detected among any of the areas when analysing samples from cluster 1 and cluster 2 separately..

Modelled larval dispersal by currents

Modelled currents at the 3500 m level used for advective dispersal simulations are strongly bathymetrically constrained, so mean flow patterns (Fig. 5) showed considerable spatial complexity. Superimposed on these mean patterns is variability induced in part by the deep penetration of passing eddies and other flow structures higher in the water column (Aleynik *et al.* 2017). The dispersal of simulated particles therefore reflects intricate stirring with a weak underlying tendency towards a net movement to the north and east (Fig. 6A–E; Supplementary Video S1). The calculated probability of the transport of larvae between sites (Table 8) revealed stronger connectivity between OMS-1A and UK-1B than between these two sites and UK-1A. In part this reflects greater separation, but also a residual flow to the east along a gentle bathymetric slope around 12.5°N tends to restrict direct transport between UK-1A and these two sites. APEI-6, while considerably less connected to the other three sites as a result of its separation distance, is nearly an order of magnitude more likely to receive larvae from UK-1A than from UK-1B or OMS-1A over a 5-year timescale (potentially representing multiple successive generations).

Discussion

No evidence of cryptic species

The extremely low variability of *COI* I3-M11 partion in samples ~900 km apart showed by *P. craigi* in our study is not surprising for sponges. The commonly used Folmer region of the *COI* gene (Folmer *et al.* 1994) has traditionally showed relatively low genetic variation within sponge species (Worheide *et al.* 2005), explained by slow mitochondrial *COI* sequence evolution in sponges, with very few exceptions (Duran & Rützler 2006; DeBiasse *et al.* 2010), possibly related to the active presence of mitochondrial repair mechanisms (Huang *et al.* 2008). Other mitochondrial partitions such as the Erpenbeck's 'I3-M11' fragment (Erpenbeck *et al.* 2006), has proven to be suitable for population connectivity studies in other sponges (e.g. López-Legentil & Pawlik 2009; Xavier *et al.* 2010), but it provided no resolution in our study (Fig. 3). Importantly, this extremely low *COI* variability was observed for samples included in cluster 1, which grouped samples collected from the APEI-6_Flat and several UK-1A sampling sites, two areas ~800 km apart that showed unexpected gene flow in our analysis (Fig. 4A–B). As for the morphology of the spicules, it is important to note that similar morphological differences in spheroxyasters from the specimens of cluster 1 and cluster 2 were already detected in the specimens used in the original description of *P. craigi* (Lim *et al.* 2017); the specimens analysed by Lim *et al.* (2017) were all collected from OMS-1A (all of them belonging to cluster 2), which indicates that the spheroxyasters of *P. craigi* display a moderate intraspecific variability. Thus, our findings of homogeneity in *COI* and *28S*, together with our analysis of spicule spheroxyasters morphology and size (Fig. 3, Supplementary Figure S1), provided no evidence for cryptic species in the samples used in our study and suggest that all the organisms used in our study belong to the same species. However, the possibility of members of cluster 1 being a cryptic species should not be ruled out. For this reason, we decided to run most of the downstream analyses considering members of cluster 1 and cluster 2 separately.

Body size in P. craigi

The significant size differences observed in the individuals of *P. craigi* collected from APEI-6 and OMS-1A compared to the ones collected in UK-1A and UK-1B (Fig. 2, Table 3) might be attributed to specimens in these areas belonging to different age cohorts or explained by ecological differences in the different areas. Under these premises, three possible scenarios are presented: (i) a relatively more recent colonization of nodules by *P. craigi* in APEI-6 and OMS-1A; (ii) population decimations of the sponge causing bottlenecks in APEI-6 and OMS-1A; and (iii) differences in food availability in the different areas. The first scenario might be plausible in the case of APEI-6, since most water and gene flow is predominantly northwards, and, therefore, the individuals in APEI-6 might be the result of a recent colonization. For OMS-1A, though, this possibility seems less likely since the suggested direction of migration originates mainly from OMS-1A into the rest of the areas. Thus this hypothesis will not explain why individuals in OMS-1A are significantly smaller than the ones in UK-1B (Table 3). On the other hand, all areas presented recent signs of bottleneck events (Supplementary Table S9), and, therefore, bottlenecks could not explain the differences in size observed among areas.

Alternatively, it seems that differences in food availability might explain differences observed between APEI-6 and UK-1A and UK-1B specimen sizes. *Plenaster craigi* is a filter-feeding organism relying on suspended particulate organic matter, bacteria and other microorganisms. The CCZ is known to have an overall westward and northward trend of reduced primary productivity in the central Pacific (Smith & Demopoulos 2003; Vanreusel *et al.* 2016), that has been suggested to yield a significant decline in the polychaete abundance when moving from the eastern to the western end (Smith *et al.* 2008b) and also to a decline of epifauna associated with manganese nodules in areas to the north (Vanreusel *et al.* 2016). In our case, smaller specimens of *P. craigi* found in the north (APEI-6) compared to those in the south (UK-1A and UK-1B) could result from differences in overlying primary productivity and export flux (Supplementary Figure S7, data extracted from Lutz *et al.* 2007). However, the reason why samples from OMS-1A (also in the south) were significantly smaller than samples from UK-1B despite being at similar latitudes (and only separated by ca. 75 km) and the little differences they show in POC flux (Supplementary Figure S7) remains unclear.

Genetic diversity in P. craigi

Mean expected heterozygosity (H_e), commonly used as a measure of genetic diversity, for all loci across all sites ranged from 0.728–0.791 between the four different areas, with similar values being reported when considering cluster 1 and cluster 2 separately. Such relatively high genetic diversity values could be correlated to either high mutation rates and/or relatively stable population sizes (Kimura 1983). In our case, all populations seemed to have similar effective population sizes and all showed signs of population bottlenecks, and, therefore, we could not confirm whether they were stable populations.

The genetic diversity values found in our study are within the range of other studies on marine sponges using microsatellite markers. Comparisons with data available in these studies (Duran *et al.* 2004; Blanquer *et al.* 2009; Blanquer & Uriz 2010; Dailianis *et al.* 2011; Guardiola *et al.* 2012, 2016; Bell *et al.* 2014; Pérez-Portela *et al.* 2015; Giles *et al.* 2015; Chaves-Fonnegra *et al.* 2015; Riesgo *et al.* 2016, under review; Padua *et al.* 2017), revealed that H_e increased as the sampling range covered larger distances (Fig. 7). Our H_e values are especially similar to those in studies covering around 1,000 km, a spatial scale similar to ours.

Even though genetic diversity reported here was high for most of the populations and all the areas (also when considering members of cluster 1 and cluster 2 separately), high positive F_{IS} values were also observed, indicating strong levels of inbreeding (*i.e.* non-random mating between individuals) in *P. craigi*. Such inbreeding signatures are also supported by the deviations from HWE observed in most populations of *P. craigi*. Signatures of Hardy Weinberg disequilibrium are often the rule in shallow-water sponges (*e.g.* Duran *et al.* 2004; Dailianis *et al.* 2011; Pérez-Portela *et al.* 2015; Giles *et al.* 2015; Chaves-Fonnegra *et al.* 2015; Riesgo *et al.* 2016) and also in the deep-water reef-forming sponge *Aphrocallistes vastus* Schulze, 1886, although in this case disequilibrium was observed only at global and regional scales and not within sites (Brown *et al.* 2017). As it has recently been discussed by Riesgo et al., (2016) and other studies, reasons explaining the high levels of homozygosity in sponge populations may include a significant effect of null alleles, high levels of inbreeding, selection against

heterozygotes, the Wahlund effect, or a combination of these (Freeland *et al.* 2011). In *P. craigi*, the effect of null alleles should be disregarded since, the four different areas still showed a significant departure from HWE (Table 2), although some of the populations showed no departure from HWE when removing the loci possibly affected by the presence of null alleles (3Ple, 10Ple, 11Ple and 19Ple). High F_{IS} values and departure from HWE in *P. craigi* are likely related to the biology of the species, as has already been claimed in other studies on shallow-water sponges (Chaves-Fonnegra *et al.* 2015; Riesgo *et al.* 2016). Very little is known about the reproduction of deep-sea sponges in general (Witte 1996), and nothing about the reproduction of *P. craigi* in particular, but we suggest that one of the main reasons behind the high levels of inbreeding and deficit of heterozygosity might be self-recruitment. This may be a result of limited dispersal of either gametes or larvae in *P. craigi*, supported by the observation that deep-sea currents in this area are weak and dispersal by currents is expected to be small between successive generations. Self-recruitment also been suggested for other marine sessile invertebrates with larvae with low-dispersal abilities, including both shallow-water (e.g. Chaves-Fonnegra *et al.* 2015; Pérez-Portela *et al.* 2016; Riesgo *et al.* 2016) and deep-sea species (Le Goff-Vitry *et al.* 2004). Finally, the Wahlund effect caused by subpopulation structure should not be ruled out as a possible reason explaining low levels of heterozygosity, since it has already been documented for sponges (Chaves-Fonnegra et al., 2015) and cnidarians (Ledoux *et al.* 2010).

Population differentiation, connectivity and the effect of oceanic circulation in P. craigi

Our microsatellite dataset provided detailed resolution of the genetic differentiation and connectivity of *P. craigi.* The populations studied here showed marked genetic structure at large geographical scales, as indicated by the significant differences observed between the four different areas in the AMOVA analysis, together with the low but significant F_{ST} values when comparing the four areas in pairwise groupings, except for the comparison between APEI-6 and UK-1A (Table 4–5). In this sense, isolation by distance (IBD) could not explain this pattern of large-scale differentiation and instead two major genetic discontinuities were detected: one

separating APEI-6 and some sites of UK-1A from the rest of sites sampled, and another one separating most of the samples from OMS-1A from the rest of areas (Supplementary Figure S5).

Baco et al., (2016) recently reviewed the incidence of IBD in deep- and shallow-water marine organisms (no sponges were included in their analysis), and they concluded that scales of dispersal and connectivity in deep-water organisms are comparable to those reported for shallow-water organisms, which would then justify comparing our results with others for shallow-water organisms. In this sense, several shallow-water sponges seem to be substantially affected by oceanographic fronts, ocean depth, and water circulation patterns, showing very little incidence of patterns following the stepping stone gene flow derived from IBD (e.g. Dailianis *et al.* 2011; Chaves-Fonnegra et al., 2015; Riesgo et al., 2016; Padua *et al.* 2017). Interestingly, no IBD was detected for a hadal amphipod species of the genus *Paralicella* occurring in the Pacific, with geological events and topographical barriers most likely responsible for the major isolation observed among their populations (Ritchie *et al.* 2017). In contrast, IBD has also commonly been reported in shallow-water sponges specially in studies comprising large-scale sampling sites (e.g. Duran, Pascual, Estoup, & Turon, 2004; Guardiola, Frotscher, & Uriz, 2016; Wörheide, Epp, & Macis, 2008) or even at smaller scales after removing from the analysis populations occurring in areas separated by well-known oceanographic barriers (Riesgo *et al.* 2016), and has commonly been explained by low dispersal abilities of sponges. There is also a wealth of examples in other shallow-water organisms showing IBD between their populations, even when considering species with presumably high dispersal abilities (e.g. Launey *et al.* 2002; Maier *et al.* 2005; Zulliger *et al.* 2009).

Testing environmental factors responsible for the genetic structure observed is a major goal in ecological analysis and, at the same time, is one of the major challenges for studies aiming to describe genetic connectivity in the deep sea (Hansen & Hemmer-Hansen 2007; Taylor & Roterman 2017). To our knowledge, the combination of ecological and physical models and population genetics has been attempted for relatively few studies of deep-sea organisms but has usually provided greater insights into the factors ultimately determining connectivity among populations (Jorde *et al.* 2015; Dambach *et al.* 2016). Our use of oceanographic models to

estimate larval transport may explain some of the patterns in the large-scale population differentiation and connectivity of *P. craigi*. The major differentiation found for the OMS-1A area (both in STRUCTURE and DAPC analyses) could be explained by the occurrence of currents and eddies mainly running northwards from OMS-1A (Fig. 5–6), thus preventing gene flow into OMS-1A from the other sampled areas, which was also observed in the analysis of the directionality of the gene flow (Figure 6F). A northward net larval transport would connect UK-1B and UK-1A, which was also corroborated by the low (although significant) F_{ST} values found between these two areas and the affinities found in the DAPC analyses.

We detected signatures of gene flow within samples from cluster 1 recovered in STRUCTURE, which grouped together samples separated ~800 km apart (*e.g.* APEI-6_Flat and UK-1A_BC08-BC05 and UK-1A_BC03), showing significant pairwise F_{ST} comparisons between this group of samples and the rest of sampling sites (Supplementary Table S5). Although relative migration may not be significant between APEI-6 and UK-1A (Fig. 6F), our particle movement model suggested larval flow mainly from UK-1A to APEI-6, potentially enabling connectivity between these two areas (Figure 6) via stepping-stone populations. Thus, despite being separated by ~800 km, individuals from these two areas assigned to cluster 1 showed closer genetic affinities between them than they did with individuals from nearby sites only 10s km apart. This evidence of population structure on 10-km scales could not be explained by our circulation model, and could be related to cryptic speciation and/or unexplained characteristics of the reproductive biology of *P. craigi* causing limited dispersal under some conditions. On the other hand, connectivity patterns over almost 1,000 km as observed between UK-1A and APEI-6 populations are not unexpected, since gene flow in the deep sea appears generally more extensive horizontally over large distances than vertically (e.g. Clague *et al.* 2012; O'Hara *et al.* 2014). However, there is no direct knowledge of the reproductive or larval biology of *P. craigi*, and our current understanding of circulation patterns near the CCZ floor remain limited, requiring caution in the interpretation of our circulation modelling.

Our migration analyses showed very little movement of individuals between areas, with less than two immigrants per generation in all cases (Table 7). Although relative migration levels

were higher from OMS-1A to the rest of the areas, from APEI-6 and UK-1A, and among UK-1A and UK-1B, in general all migration levels were very low (Table 6). This suggests that sponge recolonization follow large-scale mining disturbance in the UK-1 and OMS contract areas may be slow due to the limitations of larval dispersal. For sponges, low migration levels between populations is not rare, since very few migrants are usually reported among locations (e.g., Riesgo et al., 2016), and this pattern is also shared with other sessile invertebrates (Pérez-Portela et al. 2015). By contrast, a deep-sea amphipod species of the genus *Paralicella* displayed a remarkably high and reciprocal Pan-Pacific migration between hadal trench populations (Ritchie *et al.* 2017). Contrasting results for *P. craigi* and the above-mentioned hadal amphipod may be explained by the fact that, as for the majority of deep-sea scavenging amphipods, members of the genus *Paralicella* are obligate necrophages with direct development and active dispersal through swimming by juveniles and adults (Van Dolah & Bird 1980).

Importance for conservation

A general consensus exists in that there is currently a very limited understanding of the communities and the species present in the deep-sea regions under the threat of major mining disturbances, which compromises our ability to manage them sustainably (Hilario *et al.* 2015). In the development of a Regional Environmental Management Plan for the CCZ, the need to establish a series of no-mining areas was developed. These areas were termed Areas of Particular Environmental Interest (APEI). APEIs have the important proposed role of protecting vulnerable habitats and their appropriate design is crucial to safeguard the biodiversity and ecosystem function present in the region (Wedding *et al.* 2013). However, to date there has been limited study in the CCZ's APEIs. There is thus an urgent need to fill fundamental science gaps in these particular regions, especially for demographic connectivity of the species in these APEIs, one of the critical parameters to be taken into account in reserve design to avoid irreversible losses after anthropogenic disturbances (e.g. Wright *et al.* 2015).

In the light of our results, a critical question to address is: does APEI-6 safeguard biodiversity and ecosystem function represented in nearby mining exploration areas such as UK-

1A, UK-1B and OMS-1A? From the *P. craigi* data, which is limited to a single-species from a single functional group, it appears that APEI-6 does serve a conservation role (there is species overlap and connectivity between UK-1A and APEI-6), but on its own may be inadequate, especially as a source of propagules, since OMS-1A exhibits population isolation with respect to the other areas and contributes the most to the exchange of genetic diversity in the region. With regard to the genetic diversity exhibited in each area, UK-1A presented the highest values, therefore, the loss of this particular population could have repercussions on the overall genetic diversity of the species. Without further data on *P. craigi* from other APEIs (e.g. APEI-9 to the south-west of the study region), it is hard to make firm recommendations, but it would appear that an APEI designation to the south and/or west of the UK, OMS, BGR (German), NORI (Nauru) and TOML (Tonga) contract areas would be valuable, potentially supporting gene flow in westerly and northerly directions. It is notable that there are no mining exploration areas in this region, and it is thus likely to be suited to APEI designation.

Funding
This work was supported jointly by the European Union Seventh Framework Programme 'Managing Impacts of Deep-sea Resource Exploitation' (MIDAS), Agreement no. 603418, the UK Seabed Resources Ltd environmental baseline study (ABYSSLINE), and the European Union's Horizon 2020 research and innovation program 'SponGES', Grant Agreement No. 679849. The Natural Environment Research Council (NERC) funded National Capability cruise on the RRS James Cook (JC120). Additional funding was made available from the Natural History Museum, London and the Swedish research council FORMAS. Funding for the development of HYCOM was provided by the National Ocean Partnership Program and the Office of Naval Research. Data assimilative products using HYCOM are funded by the U.S. Navy. Computer time was made available by the DoD High Performance Computing Modernization Program. The output is publicly available at http://hycom.org.

Acknowledgments
The authors would like to acknowledge the outstanding support of the master and crews of the research vessels RV *Melville*, RV *Thomas G Thompson*, RRS *James Cook*. The important contribution of Magdalena Georgieva, Madeleine Brasier, Diva Amon, Iris Altamira, James Bell, Claire Laguionie, Erik Simon-Lledo, Jennifer Durden, Clemence Caulle and Veerle Huvenne in sorting samples at sea for the NHM team is gratefully acknowledged. Tom Pennance is greatly acknowledged for his assistance and advice in data analysis using Geneious. Special thanks are given to Martín Taboada Riesgo for his support during manuscript writing and also to the staff at the NHM Molecular Facilities and the Imaging and Analytical Centre for their help and advice. Three anonymous reviewers provided helpful comments and suggestions on an early version of the manuscript.

References

Aleynik DA, Inall ME, Dale AC, Vink A (2017) Impact of remotely generated eddies on plume dispersion at abyssal mining sites in the Pacific. *Nature Scientific Reports*, **7**, 16959.

Amon DJ, Ziegler AF, Dahlgren TG *et al.* (2016) Insights into the abundance and diversity of abyssal megafauna in a polymetallic-nodule region in the eastern Clarion-Clipperton Zone. *Scientific reports*, **6**, 30492.

Baco AR, Etter RJ, Ribeiro PA *et al.* (2016) A synthesis of genetic connectivity in deep-sea fauna and implications for marine reserve design. *Molecular Ecology*, **25**, 3276–3298.

Bell JJ, Smith D, Hannan D *et al.* (2014) Resilience to disturbance despite limited dispersal and self-recruitment in tropical barrel sponges: implications for conservation and management (R Pronzato, Ed,). *PLoS ONE*, **9**, e91635.

Benjamini Y, Yekutieli D (2001) The control of the false discovery rate in multiple testing under dependency. *Annals of Statistics*, **29**, 1165–1188.

Blanquer A, Uriz MJ (2010a) Population genetics at three spatial scales of a rare sponge living in fragmented habitats. *BMC Evolutionary Biology*, **10**, 13.

Blanquer A, Uriz MJ (2010b) Population genetics at three spatial scales of a rare sponge living in fragmented habitats. *BMC Evolutionary Biology*, **10**, 13.

Blanquer A, Uriz MJ, Caujapé-Castells J (2009) Small-scale spatial genetic structure In Scopalina lophyropoda, an encrusting sponge with philopatric larval dispersal and frequent fission and fusion events. *Marine Ecology Progress Series*, **380**, 95–102.

Borowski C, Thiel H (1998) Deep-sea macrofaunal impacts of a large-scale physical disturbance experiment in the Southeast Pacific. *Deep-Sea Research Part II: Topical Studies in Oceanography*, **45**, 55–81.

Brown RR, Davis CS, Leys SP (2017) Clones or clans: the genetic structure of a deep-sea sponge, *Aphrocallistes vastus*, in unique sponge reefs of British Columbia, Canada. *Molecular Ecology*, **26**, 1045–1059.

Cabranes C, Fernandez-Rueda P, Martinez JL (2007) Genetic structure of *Octopus vulgaris* around the Iberian Peninsula and Canary Islands as indicated by microsatellite DNA variation. *ICES Journal of Marine Science*, **65**, 12–16.

Chapuis M-P, Estoup A (2006) Microsatellite null alleles and estimation of population differentiation. *Molecular Biology and Evolution*, **24**, 621–631.

Chassignet EP, Hurlburt HE, Smedstad OM *et al.* (2007) The HYCOM (HYbrid Coordinate Ocean Model) data assimilative system. *Journal of Marine Systems*, **65**, 60–83.

Chaves-Fonnegra A, Feldheim KA, Secord J, Lopez J V. (2015) Population structure and dispersal of the coral-excavating sponge *Cliona delitrix*. *Molecular Ecology*, **24**, 1447–1466.

Clague GE, Jones WJ, Paduan JB, Clague DA, Vrijenhoek RC (2012) Phylogeography of *Acesta* clams from submarine seamounts and escarpments along the western margin of North America. *Marine Ecology*, **33**, 75–87.

Clement M, Posada D, Crandall K (2000) TCS: a computer program to estimate gene genealogies. *Molecular ecology*.

Cornuet JM, Luikart G (1996) Description and power analysis of two tests for detecting recent population bottlenecks from allele frequency data. *Genetics*, **144**, 2001–2014.

Dailianis T, Tsigenopoulos CS, Dounas C, Voultsiadou E (2011) Genetic diversity of the imperilled bath sponge *Spongia officinalis* Linnaeus, 1759 across the Mediterranean Sea: Patterns of population differentiation and implications for taxonomy and conservation. *Molecular Ecology*, **20**, 3757–3772.

Dambach J, Raupach MJ, Leese F, Schwarzer J, Engler JO (2016) Ocean currents determine functional connectivity in an Antarctic deep-sea shrimp. *Marine Ecology*, **37**, 1336–1344.

DeBiasse MB, Richards VP, Shivji MS (2010) Genetic assessment of connectivity in the common reef sponge, *Callyspongia vaginalis* (Demospongiae: Haplosclerida) reveals high population structure along the Florida reef tract. *Coral Reefs*, **29**, 47–55.

Van Dolah RF, Bird E (1980) A comparison of reproductive patterns in epifaunal and infaunal gammaridean amphipods. *Estuarine and Coastal Marine Science*, **11**, 593–604.

Duran S, Pascual M, Estoup A, Turon X (2004) Strong population structure in the marine

sponge *Crambe crambe* (Poecilosclerida) as revealed by microsatellite markers. *Molecular Ecology*, **13**, 511–522.
Duran S, Rützler K (2006) Ecological speciation in a Caribbean marine sponge. *Molecular Phylogenetics and Evolution*, **40**, 292–297.
Earl DA, vonHoldt BM (2012) STRUCTURE HARVESTER: A website and program for visualizing STRUCTURE output and implementing the Evanno method. *Conservation Genetics Resources*, **4**, 359–361.
Erpenbeck D, Hooper JNA, Wörheide G (2006) CO1 phylogenies in diploblasts and the "Barcoding of Life" - Are we sequencing a suboptimal partition? *Molecular Ecology Notes*, **6**, 550–553.
Evanno G, Regnaut S, Goudet J (2005) Detecting the number of clusters of individuals using the software structure: a simulation study. *Molecular Ecology*, **14**, 2611–2620.
Excoffier L, Laval G, Schneider S (2005) Arlequin (version 3.0): An integrated software package for population genetics data analysis. *Evolutionary Bioinformatics Online*, **1**, 47–50.
Folmer O, Black M, Hoeh W, Lutz R, Vrijenhoek R (1994) DNA primers for amplification of mitochondrial cytochrome c oxidase subunit I from diverse metazoan invertebrates. *Molecular Marine Biology and Biotechnology*, **3**, 294–299.
Freeland JR, Kirk H, Petersen S (2011) *Molecular Ecology* (W-B UK., Ed,).
Giles EC, Saenz-Agudelo P, Hussey NE, Ravasi T, Berumen ML (2015) Exploring seascape genetics and kinship in the reef sponge *Stylissa carteri* in the Red Sea. *Ecology and Evolution*, **5**, 2487–2502.
Giribet G, Edgecombe GD, Wheeler WC, Babbitt C (2002) Phylogeny and systematic position of Opiliones: a combined analysis of Chelicerate relationships using morphological and molecular Data. *Cladistics*, **18**, 5–70.
Glover A, Dahlgren T, Wiklund H, Mohrbeck I, Smith C (2015) An end-to-end DNA taxonomy methodology for benthic biodiversity survey in the Clarion-Clipperton Zone, Central Pacific abyss. *Journal of Marine Science and Engineering*, **4**, 2.
Glover AG, Smith CR (2003) The deep-sea floor ecosystem: current status and prospects of anthropogenic change by the year 2025. *Environmental Conservation*, **30**, S0376892903000225.
Glover AG, Smith CR, Paterson GLJ *et al.* (2002) Polychaete species diversity in the central Pacific abyss: local and regional patterns, and relationships with productivity. *Marine Ecology Progress Series*, **240**, 157–169.
Le Goff-Vitry MC, Pybus OG, Rogers AD (2004) Genetic structure of the deep-sea coral *Lophelia pertusa* in the northeast Atlantic revealed by microsatellites and internal transcribed spacer sequences. *Molecular Ecology*, **13**, 537–549.
Guardiola M, Frotscher J, Uriz MJ (2012) Genetic structure and differentiation at a short-time scale of the introduced calcarean sponge *Paraleucilla magna* to the western Mediterranean. *Hydrobiologia*, **687**, 71–84.
Guardiola M, Frotscher J, Uriz M-J (2016) High genetic diversity, phenotypic plasticity, and invasive potential of a recently introduced calcareous sponge, fast spreading across the Atlanto-Mediterranean basin. *Marine Biology*, **163**, 123.
Guerard E, Manni F (2004) Manual of the user-Barrier version 2.2. *Mind*, 0–31.
Hansen M, Hemmer-Hansen J (2007) Landscape genetics goes to sea. *Journal of Biology*, **6**, 6.
Hilario A, Metaxas A, Gaudron SM *et al.* (2015) Estimating dispersal distance in the deep sea: challenges and applications to marine reserves. *Frontiers in Marine Science*, **2**, 6.
Huang D, Meier R, Todd PA, Chou LM (2008) Slow mitochondrial COI sequence evolution at the base of the metazoan tree and its implications for DNA barcoding. *Journal of Molecular Evolution*, **66**, 167–174.
Jakobsson M, Rosenberg NA (2007) CLUMPP: A cluster matching and permutation program for dealing with label switching and multimodality in analysis of population structure. *Bioinformatics*, **23**, 1801–1806.
Janssen A, Kaiser S, Meißner K *et al.* (2015) A reverse taxonomic approach to assess macrofaunal distribution patterns in abyssal Pacific polymetallic nodule fields (J Hewitt,

Ed,). *PLOS ONE*, **10**, e0117790.
Jombart T (2008) Adegenet: A R package for the multivariate analysis of genetic markers. *Bioinformatics*, **24**, 1403–1405.
Jones DOB, Kaiser S, Sweetman AK *et al.* (2017) Biological responses to disturbance from simulated deep-sea polymetallic nodule mining. *PLOS ONE*, **12**, e0171750.
Jorde PE, Søvik G, Westgaard J-I *et al.* (2015) Genetically distinct populations of northern shrimp, Pandalus borealis, in the North Atlantic: adaptation to different temperatures as an isolation factor. *Molecular Ecology*, **24**, 1742–1757.
Katoh K, Misawa K, Kuma K, Miyata T (2002) MAFFT: a novel method for rapid multiple sequence alignment based on fast Fourier transform. *Nucleic Acids Research*, **30**, 3059–3066.
Kearse M, Moir R, Wilson A *et al.* (2012) Geneious Basic: An integrated and extendable desktop software platform for the organization and analysis of sequence data. *Bioinformatics*, **28**, 1647–1649.
Kimura M (1983) *The Neutral Theory of Molecular Evolution*.
Kuhner MK (2006) LAMARC 2.0: maximum likelihood and Bayesian estimation of population parameters. *Bioinformatics*, **22**, 768–770.
Launey S, Ledu C, Boudry P, Bonhomme F, Naciri-Graven Y (2002) Geographic structure in the european flat oyster (*Ostrea edulis* L.) as revealed by microsatellite polymorphism. *Journal of Heredity*, **93**, 331–351.
Ledoux J-B, Garrabou J, Bianchimani O *et al.* (2010) Fine-scale genetic structure and inferences on population biology in the threatened Mediterranean red coral, *Corallium rubrum*. *Molecular Ecology*, **19**, 4204–4216.
Lim S-C, Wiklund H, Glover AG, Dahlgren TG, Koh-Siang T (2017) A new genus and species of abyssal sponge commonly encrusting polymetallic nodules in the Clarion-Clipperton Zone, East Pacific Ocean. *Systematics and Biodiversity*, **15**, 507–519.
Lodge M, Johnson D, Le Gurun G *et al.* (2014) Seabed mining: International Seabed Authority environmental management plan for the Clarion-Clipperton Zone. A partnership approach. *Marine Policy*, **49**, 66–72.
López-Legentil S, Pawlik JR (2009) Genetic structure of the Caribbean giant barrel sponge *Xestospongia muta* using the I3-M11 partition of COI. *Coral Reefs*, **28**, 157–165.
Luikart G, Cornuet JM (1998) Empirical evaluation of a test for identifying recently bottlenecked populations from allele frequency data. *Conservation Biology*, **12**, 228–237.
Lutz MJ, Caldeira K, Dunbar RB, Behrenfeld MJ (2007) Seasonal rhythms of net primary production and particulate organic carbon flux to depth describe the efficiency of biological pump in the global ocean. *Journal of Geophysical Research: Oceans*, **112**.
Maier E, Tollrian R, Rinkevich B, Nürnberger B (2005) Isolation by distance in the scleractinian coral *Seriatopora hystrix* from the Red Sea. *Marine Biology*, **147**, 1109–1120.
Maldonado M (2006) The ecology of the sponge larva. *Canadian Journal of Zoology*, **84**, 175–194.
Meirmans PG, Van Tienderen PH (2004) GENOTYPE and GENODIVE: Two programs for the analysis of genetic diversity of asexual organisms. *Molecular Ecology Notes*, **4**, 792–794.
Mewes K, Mogollón JM, Picard A *et al.* (2014) Impact of depositional and biogeochemical processes on small scale variations in nodule abundance in the Clarion-Clipperton Fracture Zone. *Deep-Sea Research Part I: Oceanographic Research Papers*, **91**, 125–141.
Miljutin DM, Miljutina MA, Arbizu PM, Galéron J (2011) Deep-sea nematode assemblage has not recovered 26 years after experimental mining of polymetallic nodules (Clarion-Clipperton Fracture Zone, Tropical Eastern Pacific). *Deep-Sea Research Part I: Oceanographic Research Papers*, **58**, 885–897.
Mullineaux LS (1987) Organisms living on manganese nodules and crusts: distribution and abundance at three North Pacific sites. *Deep Sea Research Part A, Oceanographic Research Papers*, **34**, 165–184.
O'Hara TD, England PR, Guasekera RM, Naughton KM (2014) Limited phylogeographic structure for five bathyal ophiuroids at continental scales. *Deep Sea Research Part I:*

Oceanographic Research Papers, **84**, 18–28.
Oebius HU, Becker HJ, Rolinski S, Jankowski JA (2001) Parametrization and evaluation of marine environmental impacts produced by deep-sea manganese nodule mining. *Deep Sea Research Part II: Topical Studies in Oceanography*, **48**, 3453–3467.
Van Oosterhout C, Hutchinson WF, Wills DPM, Shipley P (2004) MICRO-CHECKER: Software for identifying and correcting genotyping errors in microsatellite data. *Molecular Ecology Notes*, **4**, 535–538.
Padua A, Cunha HA, Klautau M (2017) Gene flow and differentiation in a native calcareous sponge (Porifera) with unknown dispersal phase. *Marine Biodiversity*, 1–11.
Paterson GLJ, Menot L, Colaço A *et al.* (2015) Biogeography and connectivity in deep-sea habitats with mineral resource potential–gap analysis. *MIDAS Deliverable 4.2*, 45.
Paterson GLJ, Wilson GDF, Cosson N, Lamont PA (1998) Hessler and Jumars (1974) revisited: abyssal polychaete assemblages from the Atlantic and Pacific. *Deep Sea Research Part II: Topical Studies in Oceanography*, **45**, 225–251.
Peakall R, Smouse PE (2006) GENALEX 6: Genetic analysis in Excel. Population genetic software for teaching and research. *Molecular Ecology Notes*, **6**, 288–295.
Peakall R, Smouse PE (2012) GenALEx 6.5: Genetic analysis in Excel. Population genetic software for teaching and research-an update. *Bioinformatics*, **28**, 2537–2539.
Pérez-Portela R, Cerro-Gálvez E, Taboada S *et al.* (2016) Lonely populations in the deep: genetic structure of red gorgonians at the heads of submarine canyons in the north-western Mediterranean Sea. *Coral Reefs*, **35**.
Pérez-Portela R, Noyer C, Becerro MA (2015) Genetic structure and diversity of the endangered bath sponge *Spongia lamella*. *Aquatic Conservation: Marine and Freshwater Ecosystems*, **25**, 365–379.
Polato NR, Concepcion GT, Toonen RJ, Baums IB (2010) Isolation by distance across the Hawaiian Archipelago in the reef-building coral *Porites lobata*. *Molecular Ecology*, **19**, 4661–4677.
Pritchard JK, Stephens M, Donnelly P (2000) Inference of population structure using multilocus genotype data. *Genetics*, **155**.
Raymond M, Rousset F (1995) GENEPOP (version 1.2): population genetics software for exact tests and ecumenicism. *Journal of Heredity*, **86**, 248–249.
Riesgo A, Maldonado M (2008) Differences in reproductive timing among sponges sharing habitat and thermal regime. *Invertebrate Biology*, **127**, 357–367.
Riesgo A, Perez-Portela R, Pita L *et al.* (2016) Population structure and connectivity in the Mediterranean sponge *Ircinia fasciculata* are affected by mass mortalities and hybridization. *Heredity*, **117**, 427–439.
Ritchie H, Jamieson AJ, Piertney SB (2017) Population genetic structure of two congeneric deep-sea amphipod species from geographically isolated hadal trenches in the Pacific Ocean. *Deep-Sea Research Part I: Oceanographic Research Papers*, **119**, 50–57.
Rosenberg NA (2004) DISTRUCT: A program for the graphical display of population structure. *Molecular Ecology Notes*, **4**, 137–138.
Rousset F (2008) GENEPOP'007: A complete re-implementation of the GENEPOP software for Windows and Linux. *Molecular Ecology Resources*, **8**, 103–106.
Schönberg CHL (2016) Effects of dredging on filter feeder communities , with a focus on sponges. Report of Theme 6 - Project 6.1 prepared for the Dredging Science Node. *Report of Theme 6 - Project 6.1.1 prepared for the Dredging Science Node, Western Australian Marine Science Institution, Perth, Western Australia. 139 pp.*, 127 pp.
Schwendinger PJ, Giribet G (2005) The systematics of the south-east Asian genus *Fangensis Rambla* (Opiliones:Cyphophthalmi:Stylocellidae). *Invertebrate Systematics*, **19**, 297.
Smith C, Demopoulos A (2003) The deep pacific ocean floor. *Ecosystems of the World*, **28**, 179–218.
Smith CR, Hoover DJ, Doan SE *et al.* (1996) Phytodetritus at the abyssal seafloor across 10° of latitude in the central equatorial Pacific. *Deep Sea Research Part II: Topical Studies in Oceanography*, **43**, 1309–1338.
Smith C, Levin L, Koslow A, Tyler P (2008a) The near future of the deep seafloor ecosystems.

In: *Aquatic ecosystems:* (ed Poulin N), pp. 334–351. Cambridge University Press, Cambridge, UK.
Smith CR, Paterson G, Lambshead J *et al.* (2008b) Biodiversity, species ranges, and gene flow in the abyssal Pacific nodule province: predicting and managing the impacts of deep seabed mining. *Project Report*.
Sundqvist L, Keenan K, Zackrisson M, Prodöhl P, Kleinhans D (2016) Directional genetic differentiation and relative migration. *Ecology and Evolution*, **6**, 3461–3475.
Taboada S, Kenny NJ, Riesgo A *et al.* (2017) Mitochondrial genome and polymorphic microsatellite markers from the abyssal sponge Plenaster craigi Lim & Wiklund, 2017: tools for understanding the impact of deep-sea mining.
Taylor ML, Roterman CN (2017) Invertebrate population genetics across Earth's largest habitat: The deep-sea floor. *Molecular Ecology*.
Thiel H, Schriever G, Ahnert A *et al.* (2001) The large-scale environmental impact experiment DISCOL—reflection and foresight. *Deep Sea Research Part II: Topical Studies in Oceanography*, **48**, 3869–3882.
Thiel H, Schriever G, Bussau C, Borowski C (1993) Manganese nodule crevice fauna. *Deep-Sea Research Part I*, **40**, 419–423.
Vanreusel A, Hilario A, Ribeiro PA, Menot L, Arbizu PM (2016) Threatened by mining, polymetallic nodules are required to preserve abyssal epifauna. *Scientific Reports*, **6**, 26808.
Veillette J, Juniper SK, Gooday AJ, Sarrazin J (2007) Influence of surface texture and microhabitat heterogeneity in structuring nodule faunal communities. *Deep-Sea Research Part I: Oceanographic Research Papers*, **54**, 1936–1943.
Vrijenhoek RC (2010) Genetic diversity and connectivity of deep-sea hydrothermal vent metapopulations. *Molecular Ecology*, **19**, 4391–4411.
Wedding LM, Friedlander AM, Kittinger JN *et al.* (2013) From principles to practice: a spatial approach to systematic conservation planning in the deep sea. *Proceedings. Biological sciences*, **280**, 20131684.
Witte U (1996) Seasonal reproduction in deep-sea sponges - triggered by vertical particle flux? *Marine Biology*, **124**, 571–581.
Wörheide G, Epp LS, Macis L (2008) Deep genetic divergences among Indo-Pacific populations of the coral reef sponge Leucetta chagosensis (Leucettidae): Founder effects, vicariance, or both? *BMC Evolutionary Biology*, **8**, 24.
Worheide G, Solé-Cava AM, Hooper JNA (2005) Biodiversity, molecular ecology and phylogeography of marine sponges: patterns, implications and outlooks. *Integrative and Comparative Biology*, **45**, 377–385.
Wright D, Bishop JM, Matthee CA, von der Heyden S (2015) Genetic isolation by distance reveals restricted dispersal across a range of life histories: Implications for biodiversity conservation planning across highly variable marine environments. *Diversity and Distributions*, **21**, 698–710.
Xavier JR, Rachello-Dolmen PG, Parra-Velandia F *et al.* (2010) Molecular evidence of cryptic speciation in the "cosmopolitan" excavating sponge Cliona celata (Porifera, Clionaidae). *Molecular Phylogenetics and Evolution*, **56**, 13–20.
Zulliger DE, Tanner S, Ruch M, Ribi G (2009) Genetic structure of the high dispersal Atlanto-Mediterreanean sea star Astropecten aranciacus revealed by mitochondrial DNA sequences and microsatellite loci. *Marine Biology*, **156**, 597–610.

Data Accessibility Statement

New *28S* and *COI* sequences were obtained and deposited in the genetic sequence database, Genbank, under the Accession numbers MH138084 - MH138092 and MH138093 - MH138157, respectively. Final genotypes are stored in the Dryad Digital Repository (doi:10.1594/PANGAEA.888006). Additional data and figures may be found in Supporting information.

Authors Contributions

S.T., H.W. C.R.S., D.O.B.J., T.G.D. and A.G.G. designed the study and collected the samples; G.L.J.P., C.R.S., D.O.B.J., T.G.D. and A.G.G. provided funding for the sampling; A.R., G.L.J.P., A.C.D., C.R.S., D.O.B.J., T.G.D. and A.G.G. contributed reagents and analytical tools; S.T., A.R., H.W., V.K. and N.S. carried out laboratory analyses; S.T. and A.R. analysed molecular data; S.T., A.R. and N.S. analysed morphological data; A.C.D. analysed oceanographic models; S.T. wrote the first draft of the paper and A.R., G.L.J.P, A.C.D., C.R.S., D.O.B.J., T.G.D. and A.G.G. made major contributions to the writing. All the authors reviewed the final version of the manuscript.

Tables

Table 1. Details of the samples analyzed in the present study at each of the sampling areas. [a] *AG* Agassiz trawl, *BC* boxcore, *EBS* epibenthic sledge, *HB* Hydraulic benthic *in situ* sampler (*Hybis* ROV), *MC* multicore. [b] In brackets the number of specimens successfully used for microsatellite analysis

Cruise/Area	Original sampling station	Gear[a]	N[b]	Depth (m)	Latitude (N)	Longitude (W)
APEI-6						
JC120	APEI-6_Flat1	BC	3 (3)	4156	17°14.448	123°0.3978
JC120	APEI-6_Flat2	BC	4 (4)	4161	17°14.9320	123°1.2820
JC120	APEI-6_Flat3	BC	6 (5)	4153	17°15.019	123°1.7570
JC120	APEI-6_Flat4	BC	2 (2)	4180	17°13.184	123°2.667
JC120	APEI-6_Flat5	BC	4 (3)	4162	17°14.381	123°1.584
JC120	APEI-6_Flat6	MC	2 (2)	4162	17°14.433	123°3.967
JC120	APEI-6_Flat7	MC	1 (1)	4155	17°15.022	123°1.759
JC120	APEI-6_Flat8	AG	2 (0)	4169	17°15.455	123°3.5890
Total Flat			**24 (20)**			
JC120	APEI-6_Ridge1	BC	3 (2)	4021	17°21.5610	122°54.185
JC120	APEI-6_Ridge2	BC	4 (2)	4045	17°18.843	122°54.047
JC120	APEI-6_Ridge3	BC	3 (2)	4028	17°22.00157	122°53.971888
JC120	APEI-6_Ridge4	BC	1 (1)	4015	17°17.31	122°53.068
JC120	APEI-6_Ridge5	BC	2 (2)	4012	17°19.672	122°53.271
JC120	APEI-6_Ridge6	MC	1 (1)	4012	17°17.30046	122°53.07351
Total Ridge			**14 (10)**			
JC120	APEI-6_Trough1	BC	1 (1)	4264	17°13.868817	122°48.90019
JC120	APEI-6_Trough2	BC	5 (2)	4231	17°17.77448	122°50.12778
JC120	APEI-6_Trough3	MC	2 (2)	4234	17°17.789	122°50.128
Total Trough			**8 (5)**			
JC120	APEI-6_Deep1	BC	1 (1)	4297	16°54.7716	122°59.8412
JC120	APEI-6_Deep2	MC	1 (1)	4297	16°54.7770	122°59.8290
JC120	APEI-6_Nodule	HB	1 (1)	4321	16°53.4309	122°50.6078
Total Deep_Nodule			**3 (3)**			
Total APEI-6			**49 (38)**			
UK-1A						
AB01	UK-1A_BC03	BC	3 (2)	4171	13°52.900	116°28.000
AB01	UK-1A_BC05	BC	17 (17)	4081	13°47.601	116°42.185
AB01	UK-1A_BC06	BC	1 (1)	4084	13°57.794	116°34.093
AB01	UK-1A_BC08	BC	1 (1)	4076	13°48.700	116°42.600
AB01	UK-1A_BC10	BC	7 (7)	4036	13°45.001	116°30.799
AB01	UK-1A_BC12	BC	8 (8)	4050	13°51.801	116°32.800
AB01	UK-1A_BC14	BC	10 (10)	4160	13°43.597	116°40.200
AB01	UK-1A_EB03	EBS	1 (1)	4130	13°57.437	116°30.101
AB01	UK-1A_EB04	EBS	3 (3)	4128	13°48.254	116°28.196
Total UK-1A			**51 (50)**			

UK-1B						
AB02	UK-1B_BC01	BC	5 (5)	4127	12°24.977	116°42.891
AB02	UK-1B_BC02	BC	2 (2)	4159	12°22.022	116°31.021
AB02	UK-1B_BC03	BC	5 (5)	4144	12°24.410	116°29.085
AB02	UK-1B_BC04	BC	1 (1)	4160	12°22.259	116°36.819
AB02	UK-1B_BC06	BC	2 (2)	4237	12°34.742	116°41.218
AB02	UK-1B_BC13	BC	2 (2)	4130	12°27.066	116°35.661
AB02	UK-1B_BC15	BC	5 (5)	4196	12°27.107	116°30.736
AB02	UK-1B_BC17	BC	3 (3)	4228	12°34.190	116°32.333
AB02	UK-1B_BC18	BC	10 (10)	4136	12°25.195	116°37.477
AB02	UK-1B_BC20	BC	3 (3)	4258	12°35.813	116°29.614
AB02	UK-1B_EB09	EBS	1 (1)	4460	12°21.62	116°41.99
AB02	UK-1B_MC13	MC	1 (1)	4129	12°27.059	116°35.667
AB02	UK-1B_MC25	MC	1 (1)	4224	12°34.953	116°39.058
Total UK-1B			**41 (41)**			
OMS-1A						
AB02	OMS-1A_BC07	BC	2 (2)	4183	12°07.066	117°20.621
AB02	OMS-1A_BC08	BC	1 (1)	4114	12°10.868	117°15.659
AB02	OMS-1A_BC09	BC	5 (5)	4070	12°04.914	117°10.691
AB02	OMS-1A_BC10	BC	2 (2)	4144	12°00.567	117°10.687
AB02	OMS-1A_BC11	BC	3 (3)	4090	12°13.0425	117°19.5229
AB02	OMS-1A_BC12	BC	4 (4)	4044	12°08.695	117°19.526
AB02	OMS-1A_BC21	BC	6 (6)	4054	12°08.156	117°12.900
AB02	OMS-1A_BC22	BC	7 (7)	4051	12°05.994	117°11.796
AB02	OMS-1A_BC23	BC	3 (3)	4095	12°03.278	117°15.103
AB02	OMS-1A_BC25	BC	3 (3)	4141	12°00.559	117°22.818
AB02	OMS-1A_BC26	BC	1 (1)	4139	12°01.643	117°19.512
AB02	OMS-1A_EB06	EBS	1 (1)	4137	12°15.05	117°19.23
AB02	OMS-1A_MC23	MC	1 (1)	4148	12°00.554	117°22.821
Total OMS-1A			**39 (39)**			
GRAND TOTAL			**180 (168)**			

Table 2. Descriptors of genetic diversity for all 30 locations and the four areas of *P. craigi* using the data set containing 11 loci and also the dataset using 7 loci after removing the four loci (3Ple, 10Ple, 11Ple and 19Ple) possibly being affected by the presence of null alleles. Some of the sampling stations are the result of pooling the original sampling stations from Table 1. *N* sample size, *Na* mean number of alleles per locus, *Pa* mean number of private alleles, *He* expected heterozygosity, *Ho* observed heterozygosity, F_{IS} inbreeding coefficient, *HWE* Significant deviation from Hardy-Weinberg Equilibrium after application of Narum correction ($P < 0.05$). ns=not significant, ** P<0.01, *** P<0.001

Area/Sampling station	N	Na		Pa		Ho		He		F_{IS}		HWE	
		11 loci	7 loci	11 loci	7 loci	11 loci	7 loci	11 loci	7 loci	11 loci	7 loci	11 loci	7 loci
APEI-6													
APEI-6_Ridge	10	6.364	5.857	0.273	0.286	0.570	0.671	0.700	0.654	0.163	-0.040	***	ns
APEI-6_Trough	5	4.727	4.143	0.000	0.000	0.564	0.571	0.658	0.597	0.167	0.084	ns	ns
APEI-6_Flat	20	10.364	9.857	0.273	0.143	0.478	0.554	0.705	0.664	0.304	0.140	***	***
APEI-6_Deep-Nodule	3	3.364	3.000	0.000	0.000	0.485	0.476	0.571	0.484	0.170	0.040	ns	ns
Total APEI-6	38	13.455	12.857	0.727	0.571	0.516	0.583	0.775	0.735	0.342	0.225	***	***
UK-1A													
UK-1A_BC06-EB03	2	2.273	2.429	0.000	0.000	0.545	0.643	0.500	0.554	-0.080	-0.143	ns	ns
UK-1A_BC08-BC05	18	8.000	7.571	0.636	0.571	0.480	0.549	0.697	0.657	0.326	0.193	***	***
UK-1A_BC12	8	6.000	5.286	0.909	1.286	0.365	0.385	0.689	0.628	0.395	0.275	***	***
UK-1A_BC03	2	2.636	2.714	0.000	0.000	0.636	0.714	0.466	0.518	-0.383	-0.400	ns	ns
UK-1A_BC14	10	6.273	6.429	0.545	0.857	0.445	0.500	0.658	0.668	0.305	0.229	***	***
UK-1A_EB04	3	2.818	2.571	0.000	0.000	0.576	0.619	0.500	0.460	-0.183	-0.343	ns	ns
UK-1A_BC10	7	5.727	5.286	0.000	0.000	0.498	0.469	0.684	0.635	0.317	0.337	***	***
Total UK-1A	50	15.636	16.000	2.364	2.857	0.472	0.513	0.791	0.760	0.412	0.340	***	***
UK-1B													
UK-1B_BC06-MC25	3	3.364	3.286	0.000	0.000	0.545	0.619	0.571	0.540	0.056	-0.140	ns	ns
UK-1B_BC17	3	3.091	2.857	0.091	0.143	0.545	0.619	0.540	0.508	-0.031	-0.259	ns	ns
UK-1B_BC20	3	3.455	3.286	0.091	0.143	0.470	0.476	0.612	0.587	0.232	0.174	ns	ns
UK-1B_BC01	5	4.091	4.143	0.182	0.143	0.491	0.571	0.595	0.571	0.186	0.019	**	ns

UK-1B_BC18-MC13	11	6.909	6.571	0.455	0.714	0.415	0.455	0.649	0.576	0.331	0.200	***	***
UK-1B_BC13	2	2.000	2.286	0.000	0.000	0.500	0.643	0.364	0.429	-0.383	-0.489	ns	ns
UK-1B_BC15	5	4.000	3.857	0.182	0.000	0.468	0.521	0.571	0.512	0.147	-0.056	ns	ns
UK-1B_EB09-BC04	2	2.455	2.286	0.000	0.000	0.500	0.571	0.523	0.482	0.093	-0.156	ns	ns
UK-1B_BC02	2	1.091	1.143	0.091	0.000	0.136	0.071	0.170	0.125	0.167	0.333	ns	ns
UK-1B_BC03	5	3.273	2.857	0.091	0.143	0.491	0.543	0.532	0.476	0.101	-0.102	ns	ns
Total UK-1B	41	13.273	13.429	1.364	1.429	0.470	0.517	0.728	0.676	0.328	0.206	***	***
OMS-1A													
OMS-1A_EB06-BC11-BC08	5	4.818	4.857	0.091	0.143	0.491	0.543	0.675	0.649	0.256	0.145	***	ns
OMS-1A_BC12	4	3.636	3.286	0.091	0.143	0.545	0.536	0.597	0.531	0.045	-0.032	ns	ns
OMS-1A_BC07	2	2.909	2.714	0.182	0.143	0.591	0.571	0.568	0.518	-0.013	-0.111	ns	ns
OMS-1A_BC21	6	5.273	5.143	0.000	0.000	0.536	0.629	0.663	0.610	0.211	0.041	***	ns
OMS-1A_BC22	7	5.455	5.571	0.455	0.714	0.409	0.449	0.620	0.582	0.317	0.170	***	ns
OMS-1A_BC09	5	4.273	4.143	0.000	0.000	0.418	0.486	0.636	0.577	0.298	0.119	***	ns
OMS-1A_BC23	3	2.545	2.571	0.182	0.286	0.515	0.524	0.455	0.429	-0.088	-0.197	ns	ns
OMS-1A_BC25-MC23-BC26	5	4.455	5.000	0.182	0.286	0.559	0.621	0.613	0.663	0.061	0.022	ns	ns
OMS-1A_BC10	2	2.364	2.286	0.091	0.143	0.682	0.857	0.511	0.500	-0.345	-0.695	ns	ns
Total OMS-1A	39	13.273	13.857	2.091	3.143	0.502	0.557	0.728	0.690	0.300	0.179	***	***
GRAND TOTAL	168	4.267	14.036	--	--	0.498	0.543	0.576	0.715	0.115	0.179	***	***

Table 3. Results of the ANOVA analyses on the maximum length of the individuals of *Plenaster craigi* from the four different areas and from individuals assigned to the cluster 1 from APEI-6 and UK-1A areas. *df* degrees of freedom, *F* F-test statistic, *F crit* F-test statistic critical value, *MS* mean square, *N* number of individuals, *S.D.* standard deviation, *SS* sum of squares. *significant value

Summary

Areas	N	Mean (µm)	S.D. (µm)
All areas			
APEI-6	48	3624	1265
UK-1A	35	4641	1529
UK-1B	41	5133	1776
OMS-1A	30	3991	1550
Selected indiv. Cluster 1			
APEI-6	16	3551	1372
UK-1A	13	4409	861

ANOVA

Source of variation	SS	df	MS	F	*p*-value	F crit
All areas						
Between Groups	57128751	3	19042917	8.15	0.00005*	2.66
Within Groups	350419781	150	2336132			
Total	407548532	153				
Selected indiv. Cluster 1						
Between Groups	5267595	1	5267595	4.60	0.04107*	4.21
Within Groups	30900318	27	1144456			
Total	36167913	28				

Table 4. F_{ST} values between pairs of areas for *P. craigi* based on 11 microsatellites. *significant values after applying the false discovery rate.

Area	APEI-6	UK-1A	UK-1B	OMS-1A
APEI-6	-----			
UK-1A	0.00709	-----		
UK-1B	**0.06346***	**0.06856***	-----	
OMS-1A	**0.11132***	**0.10801***	**0.07711***	-----

Table 5. Results of the Analysis of Molecular Variance (AMOVA) between the four different areas (APEI-6, UK-1A, UK-1B and OMS-1A). *significant values

Source of variation	**d.f.**	**Sum of squares**	**% variation**	**Fixation indices**	***P*-value**
Among areas	3	38,317	5.09	FCT = 0.05089	**0.04665***
Among populations within areas	26	96,045	8.84	FSC = 0.09314	**0.00000***
Among individuals within populations	138	281,648	24.9	FIS = 0.28931	**0.00000***
Within individuals	168	189	61.17	FIT = 0.38830	**0.00000***

Table 6. Asymmetric migration rates and Theta (Θ) inferred in Lamarc for *P. craigi*, with 95% credibility intervals (CIs) in brackets. Values are given for all pairwise comparisons among areas and also for areas from cluster 1.

		Migration FROM				
		APEI-6	**UK-1A**	**UK-1B**	**OMS-1A**	**Θ MPE (95% CI)**
Migration TO	**APEI-6**	-----	0.029741 (0.0565–100.0634)	0.023417 (0.03075–54.0640)	0.673238 (0.1285–2.9865)	9.754 (1.1513–10.1146)
	UK-1A	0.060954 (0.0212–99.4550)	-----	0.094908 (0.1889–23.1797)	0.031797 (0.0748–98.6775)	9.982 (0.4315–10.0744)
	UK-1B	0.037368 (0.02336–0.9680)	0.206768 (0.0835–99.1444)	-----	0.031205 (0.0356–1.7503)	9.938 (0.4435–10.3329)
	OMS-1A	0.152319 (0.5496–98.7647)	0.140648 (0.0263–99.0018)	0.121937 (0.0282–80.6290)	-----	9.896 (1.2072–10.0198)

Cluster 1		**APEI-6**	**UK-1A**	**Θ MPE (95% CI)**
	APEI-6	-----	0.054573 (-0.0827–99.4804)	9.911322 (1.4668–10.0467)
	UK-1A	0.049394 (0.0539–27.2686)	-----	9.218427 (1.5327–10.031)

Table 7. Number of immigrants per generation (ΘM) between areas for *P. craigi.* Values are given for all pairwise comparisons among areas and also for areas from cluster 1.

		Migration FROM			
		APEI-6	**UK-1A**	**UK-1B**	**OMS-1A**
Migration TO	**APEI-6**	-----	0.07	0.06	1.63
	UK-1A	0.15	-----	0.24	0.35
	UK-1B	0.09	0.51	-----	0.30
	OMS-1A	0.38	0.08	0.08	-----
Cluster 1		**APEI-6**	**UK-1A**		
	APEI-6	-----	0.11		
	UK-1A	0.14	-----		

Table 8. Connectivity matrix between the four sites derived from particle transport simulations, representing the probability that a particle transported passively from one site passes within a 25 km radius of a second site within a timescale of 5 years.

		Source site			
		APEI-6	**UK-1A**	**UK-1B**	**OMS-1A**
Receiving site	**APEI-6**	-----	0.016	0.002	0.002
	UK-1A	0.00015	-----	0.177	0.157
	UK-1B	0.00020	0.157	-----	0.254
	OMS-1A	0.00019	0.076	0.426	-----

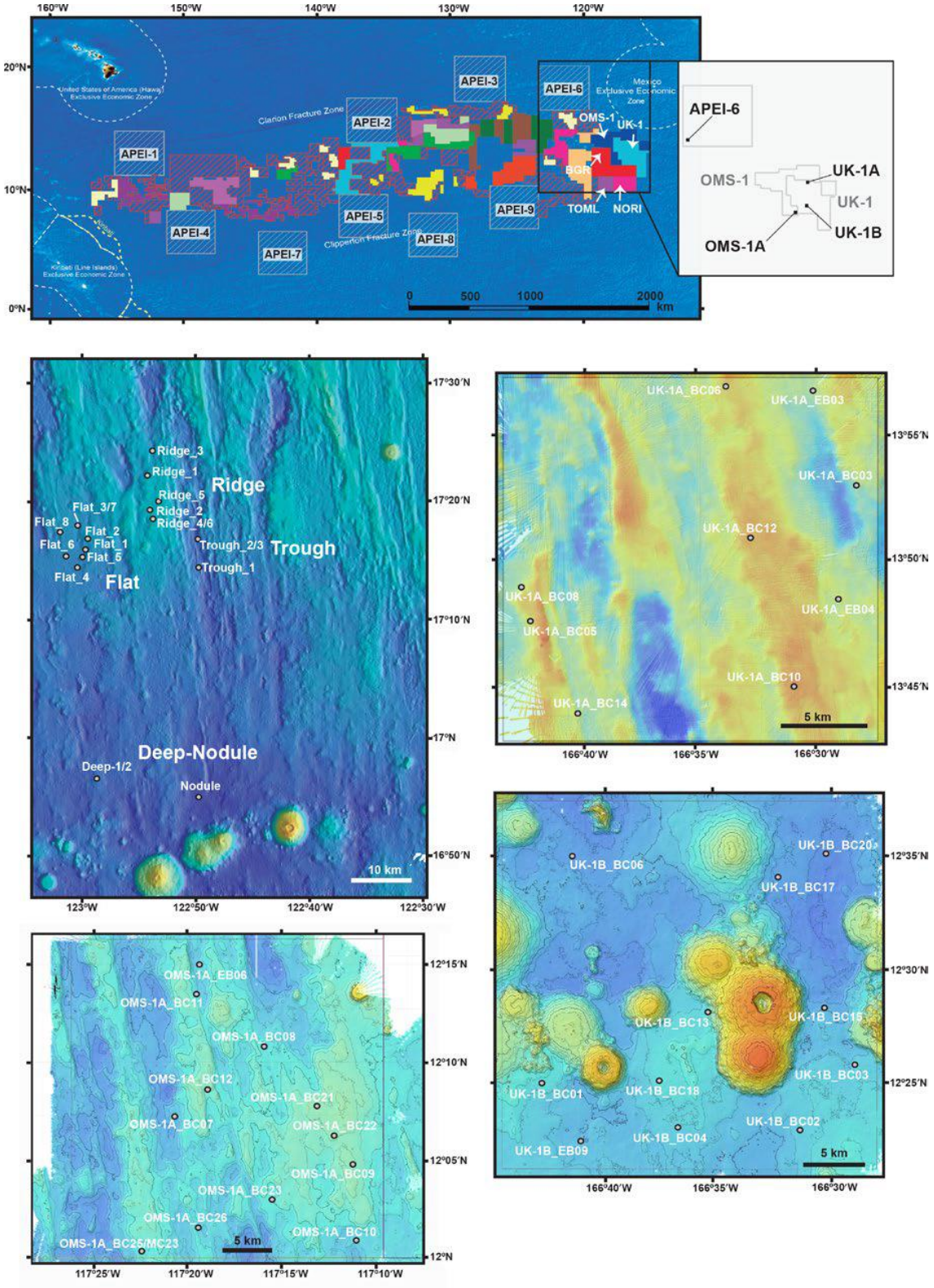

Figure 1. Map of the study area. **A** Map of the CCZ with the mining exploration areas and the network of APEI's. Inset showing the approximate position of the four different areas studied (APEI-6, UK-1A, UK-1B, and OMS-1A) **B** Detail of the APEI-6 identifying the different sampling stations in the area (Ridge_1-6, Trough_1-3, Flat_1-8, Deep_1-2, and Nodule). **C** Detail of the UK-1A identifying the different sampling stations in the area. **D** Detail of the UK-1B identifying the different sampling stations in the area. **E** Detail of the OMS-1A identifying the different sampling stations in the area.

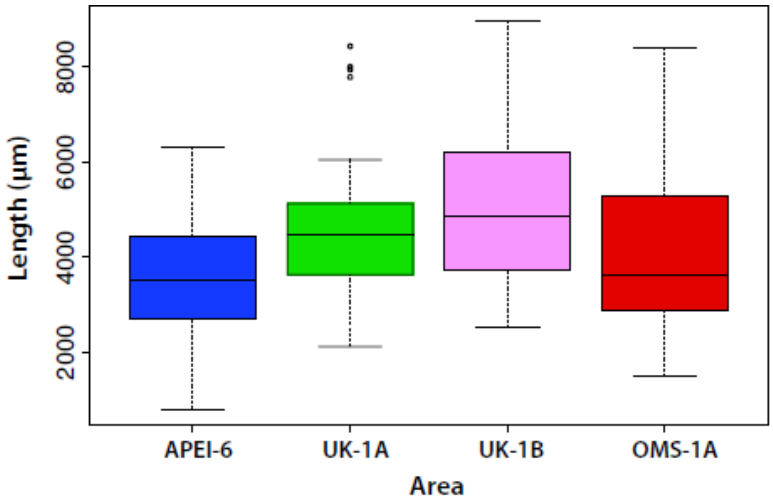

Figure 2. Mean and standard deviation of the maximum length of the individuals of *P. craigi* measured in the different areas.

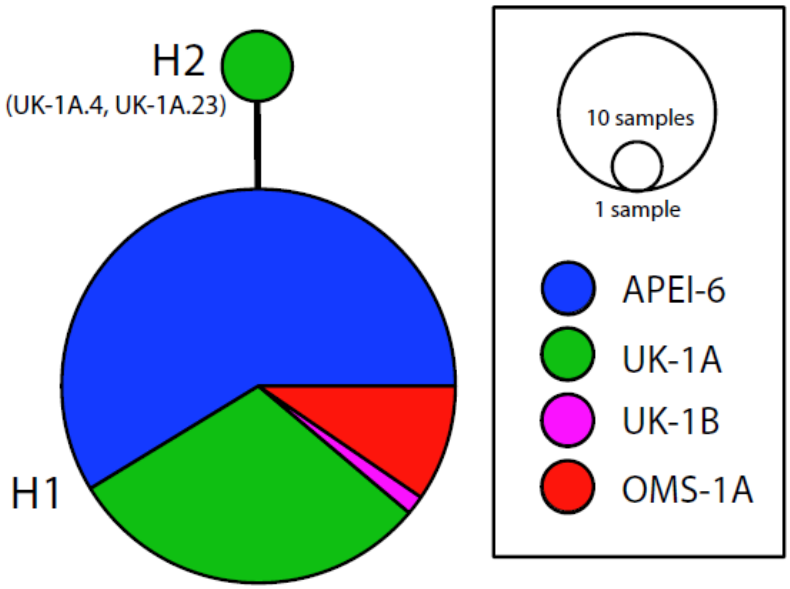

Figure 3. *COI* haplotype network for *P. craigi*. Circles are proportional to the number of individuals for each haplotype. Colour coding refers to the different areas where samples were collected.

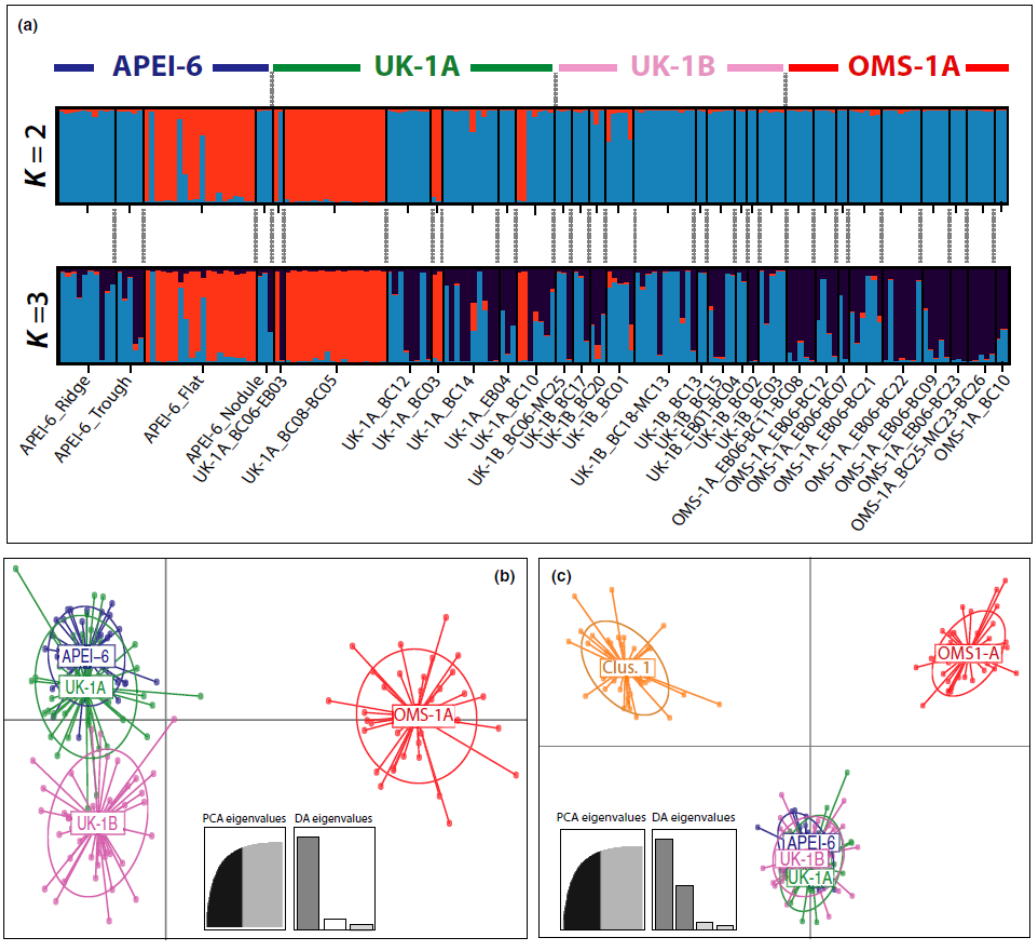

Figure 4. A Individual genotype assignment of *P. craigi* to clusters (K) as inferred by STRUCTURE for all studied sites with k = 2 and k = 3. In orange the individuals belonging to cluster 1. **B** DAPC analysis with all samples grouped in the four different areas. **C** DAPC analysis with all samples grouped in the four different areas treating apart samples from cluster 1.

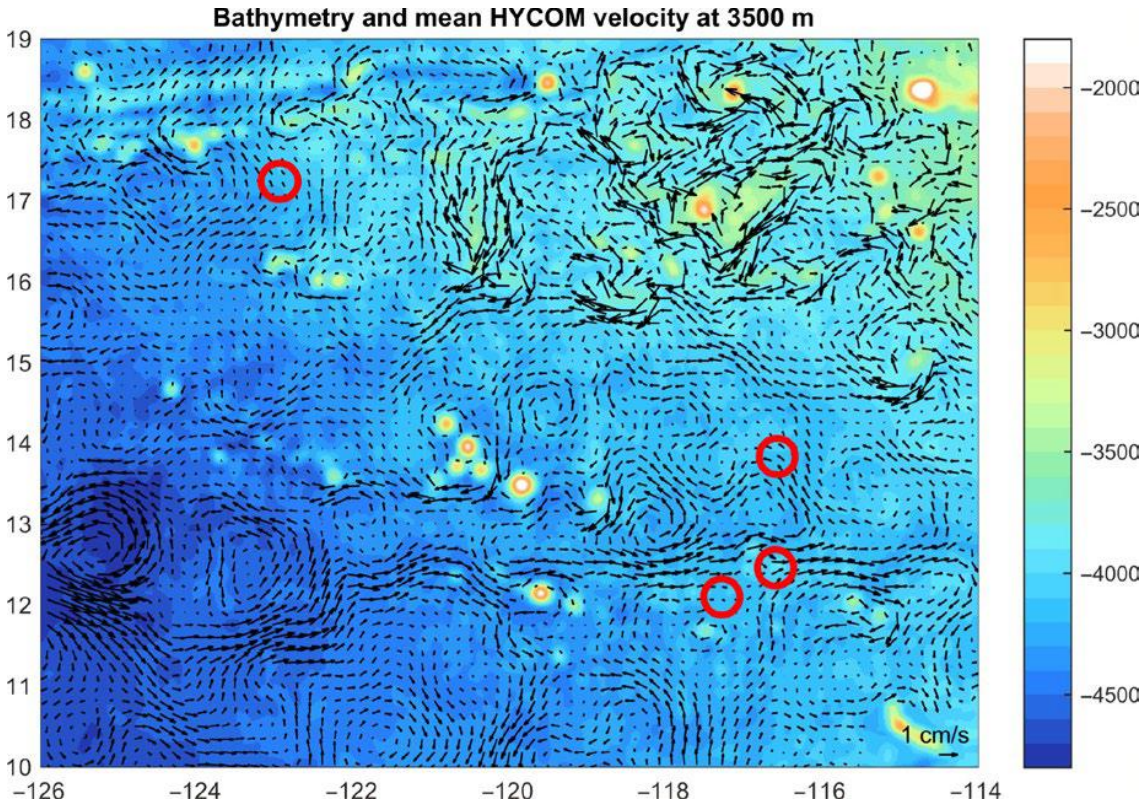

Figure 5. Mean flow at 3500 m from HYCOM simulations averaged over the 9-year period used for dispersal simulations, 10/2008 to 9/2017. The underlying image is of the model bathymetry and red circles show the 25 km radius receiving circles used for APEI-6, UK-1A, UK-1B and OMS-1A.

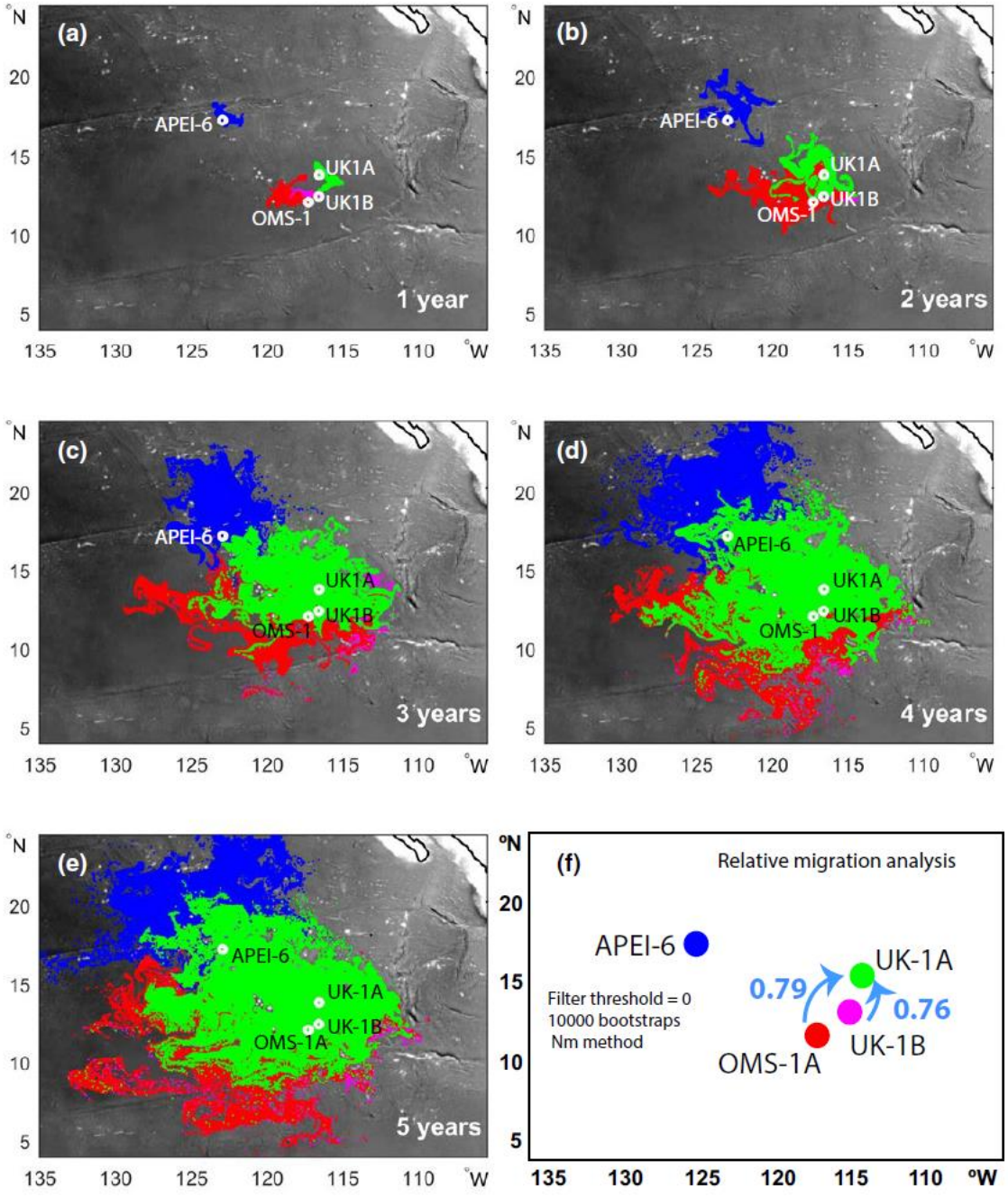

Figure 6. The distribution of particles after 1, 2, 3, 4 and 5 years (**A–E**) of continuous release and passive transport from APEI-6, UK-1A, UK-1B and OMS-1A subject to HYCOM velocities at 3500 m. **F** Migration directionality between the different areas as inferred by diveRsity. Only relative migration from UK-1B to UK-1A and from OMS-1A to UK-1A resulted significant.

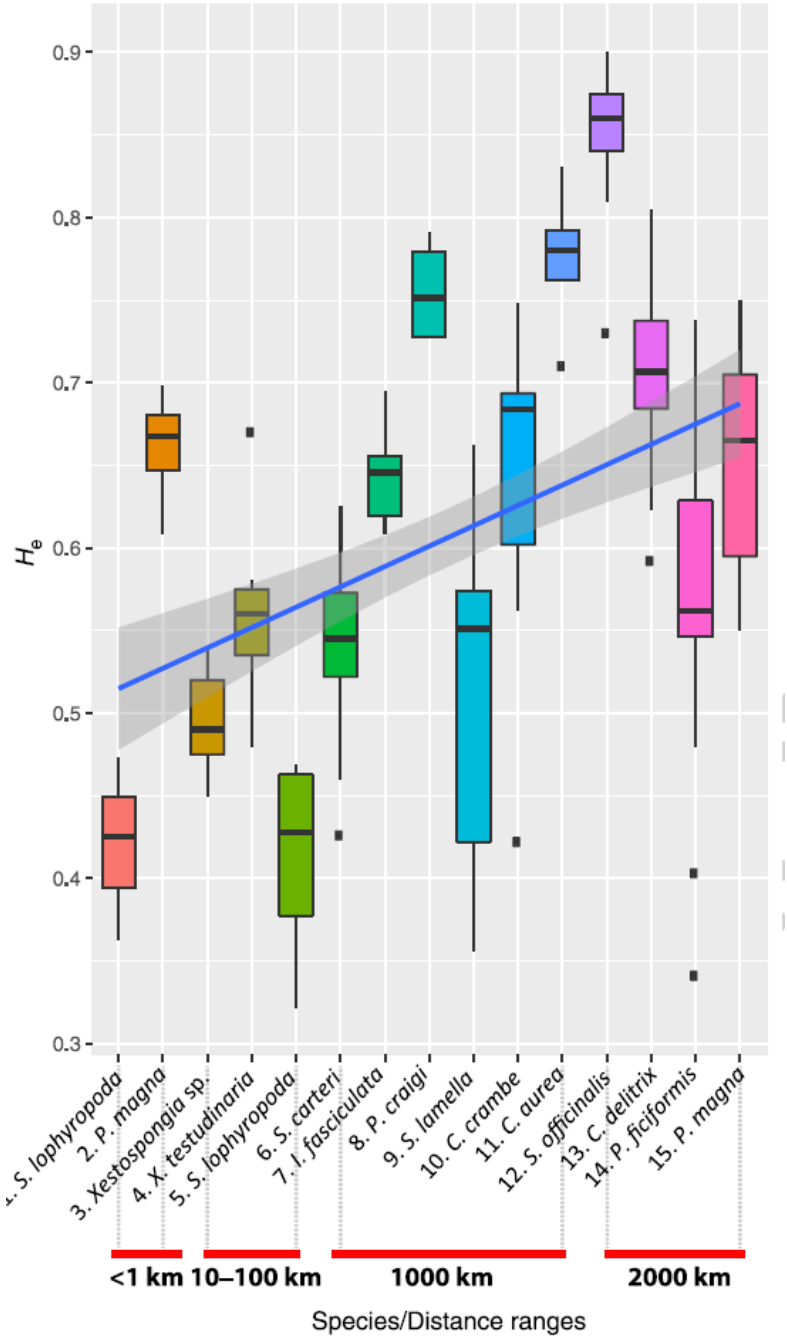

Figure 7. Genetic diversity (*He*) correlation between sponges studied using microsatellite markers. Sponges were grouped in ranges of distances (<1 km, 10–100 km, 1000 km, 2000 km) in order to make results comparable among species. 1. *Scopalina lophryopoda* (Blanquer *et al.* 2009); 2. *Paraleucilla magna* (Guardiola *et al.* 2012); 3. *Xestospongia* sp. (Bell *et al.* 2014); 4. *Xestospongia testudinaria* (Bell et al., 201; 5. *Scopalina lophryopoda* (Blanquer & Uriz 2010b); 6. *Stylissa carteri* (Giles *et al.* 2015); 7. *Ircinia fasciculata* (Riesgo *et al.* 2016); 8. *Plenaster craigi* (this study); 9. *Spongia lamella* (Pérez-Portela et al., 2015); 10. *Crambe crambe* (Duran et al., 2004); 11. *Clathrina aurea* (Padua *et al.* 2017); 12. *Spongia officinalis* (Dailianis *et al.* 2011); 13. *Cliona delitrix* (Chaves-Fonnegra *et al.* 2015); 14. *Petrosia ficiformis* (Riesgo et al., under review); 15. *Paraleucilla magna* (Guardiola *et al.* 2016).